TECHNICAL NOTES

NATIONAL ADVISORY COMMITTEE FOR AERONAUTICS

3 1176 00114 7769

No. 775

ANALYSIS OF WIND-TUNNEL DATA ON DIRECTIONAL STABILITY AND CONTROL

By H. R. Pass
Langley Memorial Aeronautical Laboratory

DOCUMENT ON LOAN FROM THE FILES OF

NATIONAL ADVISORY COMMITTEE FOR AERONAUTICS

Washington
September 1940

NATIONAL ADVISORY COMMITTEE FOR AERONAUTICS

TECHNICAL NOTE NO. 775

ANALYSIS OF WIND-TUNNEL DATA ON DIRECTIONAL STABILITY AND CONTROL

By H. R. Pass

SUMMARY

Available wind-tunnel data on static directional stability and control have been collected and studied. Methods based on these studies are given for evaluating the aerodynamic characteristics of vertical tail surfaces and their contribution to static directional stability and control. Special attention has been paid to the end-plate effect of the horizontal tail on the vertical tail and to the sidewash induced by the fuselage and the trailing vortex system from the wing. Methods based on limited data for fuselages and hulls, wings, and fuselage-wing combinations are also given for estimating the contribution of the wing and the fuselage to directional stability.

This paper does not attempt to establish criterions for directional stability and control; rather, the emphasis is placed on providing some basis for design to specified criterions. An example applying the design methods has been included.

INTRODUCTION

As a part of a general investigation directed toward developing a rational system of tail design, a study has been made of available wind-tunnel data on directional stability and control. The main emphasis has been placed on a study of the aerodynamic characteristics of the vertical tail surfaces and their contribution to the static stability and control characteristics of airplanes. Data on the characteristics of yawed fuselages, hulls, wings, wing-fuselage combinations, and wing-hull combinations have also been collected. The purpose of this study has been not to establish the stability and control criterions for satisfactory flight handling characteristics but rather to provide methods for design to specified criterions.

Rudder-effectiveness data were available for 4 airplanes and 28 models, including two 35-foot-span models of multiengine airplanes. The contribution of the vertical tail to stability, that is, yawing moments for both tail-attached and tail-removed conditions, was available for eight of these models. Yawing-moment data for fuselages and hulls were available for 17 models. For 4 of the 17 models, yaw tests had also been made of the wing alone and of the wing-fuselage combination.

The study of the forces on the vertical tail is an extension of the work of references 1 and 2, which concern the horizontal tail, and considerable use has been made of the methods that they present. Analyses were thus directed toward the determination of the characteristics of the isolated tail surface and the effective velocity and the direction of the air flow at the tail. Analyses of the yawing moments of the wing-fuselage combinations were, in general, much less satisfactory, owing to the inadequacy of methods for evaluating either the contribution of the fuselage and the wing or of the large wing-fuselage interference effects.

AIRPLANES AND MODELS

Two-view drawings of the 4 airplanes and the 28 models are given in figure 1. Many diverse types are represented, most of them of recent design. The geometric characteristics are listed in table I.

Models 1 and 2 and airplanes 3 to 6 were tested in the NACA full-scale wind tunnel; models 7 to 10, in the NACA 20-foot wind tunnel; models 11 to 16, in the NACA 7- by 10-foot wind tunnel; and models 16 to 32, in the Wright Field 5-foot wind tunnel.

AIRFOIL THEORY APPLIED TO THE VERTICAL TAIL

Considerable uncertainty attends the application of the usual airfoil theory to the design of vertical tails, owing to their low aspect ratio, the necessarily arbitrary methods of defining the area, and the large aerodynamic effects of the fuselage and the horizontal tail. Furthermore, the air flow in the region of the vertical tail may

be very irregular, particularly when the airplane is yawed, because of the low velocities in the wakes of the wing and the fuselage and the vorticity in the air flow due to the trailing-vortex system. These factors are separately discussed with the purpose of developing consistent methods of taking them into consideration.

Symbols

A	aspect ratio
b	span
L	fuselage length
l	distance from center of gravity of model to the rudder hinge line.
S	area
F_i	fuselage-wing interference factor
V	velocity
q	effective dynamic pressure at tail
q/q_o	ratio of effective dynamic pressure at tail to free-stream dynamic pressure
ρ	density
$dC_n'/d\delta_r$	rudder effectiveness
τ	relative rudder effectiveness $\left(\frac{dC_{N_t}}{d\delta_r}\Big/\frac{dC_{N_t}}{d\alpha_t}\right)$
$\bar{c}$	mean chord
C_N	normal-force coefficient
C_n'	yawing-moment coefficient (wind axes)
T_c	thrust coefficient $\left(\frac{\text{effective thrust}}{\rho V^2 D^2}\right)$

D propeller diameter

α angle of attack, degrees

ψ' angle of yaw, degrees (wind axes)

σ local sidewash angle measured from the wind axis, negative when it increases the angle of attack of the yawed vertical tail, degrees

δ deflection of movable surface, degrees

C_h hinge-moment coefficient $\left(\frac{\text{hinge moment}}{qS_r\,\bar{c}_r}\right)$

Y_f cross-wind force of fuselage

C_{Y_f}' cross-wind force coefficient of fuselage $\left(\frac{Y_f}{q\ \text{vol}^{2/3}}\right)$

u, v coefficients of C_{n_t} and δ_r in the hinge-moment equation

Subscripts:

t vertical tail

r rudder, excluding balance

b balance

f fuselage

w wing

A airplane

av average

Definitions of Geometric Characteristics

The usual vertical tail surfaces fall into five fairly well-defined groups. An example of each is shown in figure 2, which also defines the span. Type I, corre-

sponding to the twin-tail construction, is most nearly a normal airfoil and its span and area are defined in the usual manner. Type II is attached to a fuselage that tapers to a point at the rear. The span and the area are both measured to the horizontal tail, which assumes the part of an end plate. Types III and V are found on fuselages that taper, not to a point, but to a vertical knife edge at the rear. The span is measured to the horizontal tail, and the area is taken as the sum of the fin area, measured to the horizontal tail, and the total movable area. For type IV with the horizontal tail mounted on the vertical tail, the span is measured to the upper surface or to the extended upper surface of the fuselage and the area is the sum of the fin area, measured to the upper surface of the fuselage, and the total movable area. These definitions may appear rather arbitrary and are perhaps no better than others that could be chosen; yet the results obtained with them were generally consistent.

Aerodynamic Characteristics of the Isolated Vertical Tail

Normal-force characteristics.- The slope of the normal-force curve, $dC_{N_t}/d\alpha_t$, is primarily a function of aspect ratio. It must be noted, however, that the horizontal tail acts as an end plate for the vertical tail, which causes the effective aspect ratio of the vertical tail to exceed its geometric value. A theoretical analysis made by members of the full-scale-tunnel staff has shown that for the usual ratios of vertical-tail span to horizontal-tail span, the increase in aspect ratio will be about 55 percent. Tests of model 7 with two different horizontal tails indicated that the span ratio is not a critical factor. In the absence of the horizontal tail, the fuselage itself probably exerts a considerable end-plate effect. Such an effect is not readily calculable although some of the tests indicated it to be quite large.

The variation of $dC_{N_t}/d\alpha_t$ with aspect ratio is shown in the curve of figure 3, which summarizes the results of reference 3 for aspect ratios smaller than 3 and those of reference 1 for aspect ratios larger than 3. The curve represents only an average of experimental results and, under certain conditions, may be somewhat inaccurate. For example, the value of $dC_{N_t}/d\alpha_t$ may be increased 5 to 10 percent by a sealed gap between the fin and the

rudder (reference 4) or may be lowered an equal amount or more by a bad gap or by an irregular plan form.

The value of the relative rudder effectiveness τ as a function of the relative rudder and balance areas is plotted in figure 4, which reproduces the curves of figure 19 of reference 2. Here again certain deviations from the curves may be expected under various conditions, for the rudder effectiveness will also depend on the spanwise distribution of the rudder area and on the nature of the gap between the fin and the rudder (reference 4). Sealing the gap may increase τ by as much as 15 percent.

Hinge-moment characteristics.- The hinge-moment coefficient of a rudder may be expressed (reference 5) as a function of the normal-force coefficient of the tail and angle of rudder deflection

$$C_{h_r} = u\ C_{N_t} + v\delta_r \tag{1}$$

The parameters u and v may be conveniently defined from the equation in the following forms:

$$u = \left(\frac{\partial C_{h_r}}{\partial C_{N_t}}\right)_{\delta_r} = \frac{dC_{h_r}}{d\alpha_t}\bigg/\frac{dC_{N_t}}{d\alpha_t} \tag{2}$$

$$v = \left(\frac{\partial C_{h_r}}{\partial \delta_r}\right)_{C_{N_t}} = \frac{dC_{h_r}}{d\delta_r} - u\frac{dC_{N_t}}{d\delta_r} = \frac{dC_{h_r}}{d\delta_r} - u\tau\frac{dC_{N_t}}{d\alpha_t} \tag{3}$$

Hinge-moment data on isolated tail surfaces without balance and with offset-hinge balance were available in references 2, 4, and 6. From these data values of u and v, at small angles of attack and rudder deflections, were determined. The results are summarized in figures 5 and 6 wherein u and v are given as functions of S_r/S_t and S_b/S_r.

The hinge moments, for a given increase in normal force, may be appreciably less than indicated by these curves if the gap between the fin and the rudder is sealed, but may be somewhat greater if the rudder nose is very blunt.

Dynamic pressure at the tail.- The lower part of the single vertical tail is generally in a region of diminished dynamic pressure caused by the fuselage boundary layer and perhaps also by the wake from the wing-fuselage junctures. Pronounced downwash, such as will exist when partial-span flaps are deflected may, however, lower this wake and change the average dynamic pressure over the tail.

Some surveys of the air flow slightly ahead of the vertical tail of airplane 4 are shown in figure 7. The boundary layer is seen to have a considerable thickness and doubtless is even thicker farther back where it passes around the base of the vertical tail. The average dynamic pressure, as determined from such surveys, is generally slightly higher than the effective dynamic pressure acting on the tail because of the influence of the adjacent undisturbed air stream. (See reference 2.) On the basis of these surveys and the results of reference 2, the effective dynamic pressure at a single vertical tail is estimated to be, on the average, for propeller-removed conditions, about 0.90 q_0. This factor may be low for a flap-down condition or for some types of flying boats having hulls that curve upward toward the rear. At angles of attack approaching the stall, the factor may decrease owing to the effect of the thickened fuselage and the wing wake (reference 7).

Twin tails are somewhat more favorably located than single tails as the wing and the nacelle wakes appear to be less detrimental to the dynamic pressure at the tail than the fuselage boundary layer. A value of $q/q_0 = 1.00$ was used in calculating the rudder effectiveness for the models with twin tails (models 3, 8, 9, 12, and 13) and gave good agreement with the experimental values. This factor should probably be reduced if the tails are located directly in the wake of large nacelles.

At high thrust coefficients, as in take-off or climb, the slipstream will appreciably increase the average dynamic pressure at the vertical tail. (Cf. fig. 7.) In this regard, the results of reference 2 indicate that the corresponding increase in rudder effectiveness $dC_n'/d\delta_r$ may be only half as much as would correspond to the increase in average dynamic pressure.

Direction of air flow at the tail.- The air velocity in the region of the vertical tail of a yawed airplane will, in general, possess a sideward component. Accordingly, the

effective angle of attack of the vertical tail will not be equal to the angle of yaw, ψ', but will be $(\psi' - \sigma)$, where σ is the sidewash angle. The sidewash angle, which may be quite large, is associated with the trailing vortex system behind yawed wings and wing-fuselage combinations. An analysis of some recent tests at the NACA 7- by 10-foot wind tunnel (references 8 and 9) indicates that the sidewash angle probably consists of several components, the tentative theory for which is given in the following paragraphs. The order of presentation corresponds to the order of importance (as indicated by calculations).

A yawed fuselage (or airship) experiences a cross-wind force, associated with which there is a vortex system similar to that of an airfoil (reference 10). A fuselage with a low wing is comparable, in this respect, with an airfoil with an end plate, and the trailing vortex system for positive angle of yaw (nose right) will be such that:

1. The fuselage wake and the air beside it flow to the left (destabilizing sidewash, comparable with the usual destabilizing downwash).

2. The air above the fuselage wake flows to the right (stabilizing sidewash).

3. The air below the intersection of the wing and fuselage wakes has practically no sidewash.

The vertical tail surface will thus, for a low-wing airplane, be mainly in the region of stabilizing sidewash. For a high-wing airplane, however, the vertical tail will be partly in the region of destabilizing sidewash and partly in the region of no sidewash.

The vortices shed behind a lifting wing rotate in such a direction that the air moves inboard above the wake (or the trailing vortex sheet) and outboard below it. If the trailing vortex sheet is assumed to be unaltered by yawing the airplane, the vertical tail of a yawed airplane will be in an inward moving stream if it is above the wake and in an outward moving stream if it is below the wake. The effect should increase with lift coefficient and decrease with aspect ratio, and it should be especially pronounced for wings with partial-span flaps deflected.

For a wing with dihedral a change in lift at the center occurs when the wing is yawed. The vortex shed from this point rotates in such a direction as to induce outflow above the wing wake and inflow below the wing wake. Calculations indicate that this effect will be relatively small.

From the foregoing discussion it will be clear that, as regards the direction of the air flow at the tail, a low-wing design is much more favorable than a high-wing design.

Moment equations.- In conformity with the preceding discussion and analysis of the forces on the vertical tail surface, the equations for the contribution of the tail to directional stability and rudder effectiveness are written as follows:

$$\left(\frac{dC_n'}{d\psi'}\right)_t = -\frac{dC_{N_t}}{d\alpha_t}\frac{S_t}{S_w}\frac{l}{b_w}\left(1 - \frac{d\sigma}{d\psi'}\right)\frac{q}{q_o} \tag{4}$$

$$\frac{dC_n'}{d\delta_r} = -\frac{dC_{N_t}}{d\alpha_t}\frac{S_t}{S_w}\frac{l}{b_w}\tau\frac{q}{q_o} \tag{5}$$

As satisfactory first approximations, the forces have been assumed to act at the rudder hinge line and the yawing moment about the aerodynamic center of the vertical tail has been neglected.

RUDDER EFFECTIVENESS

Curves of yawing-moment coefficient against rudder angle for high-speed angles of attack are plotted in figure 8, which is divided into four parts for clarity. It may be noted that, although most of the tail surfaces do not stall in the range of rudder angles below 20°, the straight parts of the curves seldom extend much beyond rudder angles of 15°. The slope through the origin, designated the rudder effectiveness, $dC_n'/d\delta_r$, has been tabulated in the last column of table II.

Comparison of experimental with calculated values of $dC_n'/d\delta_r$.- In order to estimate the accuracy of the theory

and the methods previously outlined, values of $dC_n'/d\delta_r$ were calculated for each case by equation (5) and compared with the experimental values. The aerodynamic factors used in the calculations are listed in table II and are here briefly reviewed.

The effective aspect ratio was found for the single tails of all types except IV (see fig. 2), by multiplying the actual aspect ratio by 1.55. For conventional twin tails, the effective aspect ratio was taken to be the same as the actual aspect ratio. The values of $dC_{N_t}/d\alpha_t$ were found from figure 3 by use of the effective aspect ratios. The values of τ were found from figure 4. Values of the effective dynamic pressure ratio at the tail q/q_o were assumed to be 0.90 for the single tails and 1.00 for the twin tails.

The last two columns of table II permit a direct comparison between the calculated and the experimental rudder effectiveness. The same comparison is made graphically in figure 9, in which the epxerimental values are plotted against the calculated ones, the solid line representing exact agreement. The agreement between the experimental and the calculated results is, on the average, as satisfactory for the models as for the airplane; scale effect is apparently negligible.

Discussion and supplementary data.- The effectiveness of the horizontal tail as an end plate is obviously lost or diminished when it is located above the fuselage-vertical tail juncture (type IV of fig. 2). Calculations were omitted from table II for the four models of this type; instead, the procedure was reversed, and the increase in effective aspect ratio was calculated from the experimental rudder effectiveness. The results are shown in the following table:

Model	6		10	23	26
	Wing position				
	1	4			
Derived factor for correcting aspect ratio	0.71	0.60	1.12	1.56	1.44

The increase is small when the horizontal tail is near the

middle of the vertical tail (models 6 and 10) and large when the horizontal tail is near the bottom (models 23 and 26).

Airplanes 4 and 6 were tested both with and without the horizontal tail (table III). For model 4, removal of the horizontal tail reduced the rudder effectiveness. The reduction was relatively small, however, as if the fuselage either to a large extent replaced the horizontal tail as an end plate or else served to add some area to the vertical tail. For airplane 6, removal of the horizontal tail increased the rudder effectiveness. The horizontal tail in this case did not serve as an end plate and contributed only unfavorable interference.

Some surveys of the air flow in the region of the vertical tail were available (reference 2) for airplane 6 (fig. 10). For the parasol-wing condition (wing position 4, fig. 10(b)), the boundary layer across the root of the tail was much thicker than for the gull-wing condition (wing position 1, fig. 10(a)). Correspondingly, the rudder effectiveness was 11 percent lower for wing position 4 than for wing position 1 (table IV). The difference is possibly associated with the rotation of the vortices shed from the wing roots because, when a diverging motion is induced in the boundary layer (fig. 10(b)), it may be expected to thicken much more rapidly than when a converging motion is induced (fig. 10(a)).

The effect of propeller operation on rudder effectiveness is shown in table IV for airplane 6 with the four wing positions. For the high thrust coefficients shown, the rudder effectiveness was approximately doubled at low angles of attack and increased still further with increasing angles of attack.

The effect of angle of attack on rudder effectiveness is shown in figure 11 for nearly all the models and airplanes. In a few cases, the effectiveness continuously decreased with increasing angle of attack; for most cases, however, it remained nearly constant up to the angle of stall.

The variation of rudder effectiveness with yaw is shown in figure 12. For single tails, the rudder effectiveness increases with yaw, probably because the fuselage boundary layer at the base of the tail decreases in thickness. No corresponding variation is observed for twin tails.

The values of rudder effectiveness for flaps up and flaps down are compared in table V. Flap deflection is seen to have negligible effect except where flap deflection induced stalling.

The given definitions of span, fin area, and rudder area seem especially arbitrary when applied to vertical tails of type III, and their use in the calculation of $dC_n'/d\delta_r$ for tails of this type would correspondingly appear to have little theoretical basis. The procedure may, however, be considered as justified by the agreement between the calculated and the experimental results. Defining the rudder area so that it includes only the part above the horizontal tail led to definitely less satisfactory agreement, as is shown by the comparison in table VI.

The results in table VII show that propeller operation affects the rudder effectiveness only when the vertical tail is situated in the slipstream. The slipstream increases the rudder effectiveness because of the increased velocity of the air flow over the vertical tail and also because of the reduced thickness of the fuselage boundary layer. (Cf. fig. 7.)

VERTICAL-TAIL EFFECTIVENESS

Data from which the contribution of the vertical tail to stability could be directly evaluated were available for only eight models. The values of $dC_n'/d\psi'$ for these models with the vertical tail both attached and removed are listed in table VIII. The model from reference 9 (fig. 13), which had no horizontal tail, had been tested with three wing positions, two dihedral angles, and with 60-percent-span split flaps both up and down.

Curves of yawing-moment coefficient against angle of yaw for 23 airplanes and models are shown in figure 14. Most of the curves are straight up to relatively large angles of yaw. The value of the slope $dC_n'/d\psi'$ at $\psi' = 0°$ is taken as the criterion for directional stability.

The variation of stability with angle of attack is shown in figure 15, and the effect of flap deflection on the directional stability of complete airplanes is shown in table IX.

From the geometric characteristics of the vertical tail surfaces of table I, their corresponding values of $dC_{N_t}/d\alpha_t$ were computed. The corresponding contribution, given by equation (4), of the vertical tail to $dC_n'/d\psi'$, q/q_o being assumed equal to 0.90 for single tails and 1.00 for twin tails and sidewash being assumed absent, is shown in table VIII in the next to the last column. An increase in aspect ratio of 55 percent was assumed in these calculations for all single vertical tail surfaces except that of reference 9 which was tested without a horizontal tail and for which an increase in aspect ratio of only 45 percent was assumed.

The rate of change of sidewash angle with angle of yaw, shown in the last column of table VIII, was calculated from the difference between the experimental and the calculated values of vertical-tail effectiveness. In the results of the tests reported in reference 9, which involved a systematic variation of wing height, flap deflection, and dihedral angle, a good correspondence with the previous discussion exists in the following particulars:

(a) Raising the wing increases the average $d\sigma/d\psi'$, decreasing stability.

(b) Deflecting the flap, which strengthens the trailing vortex sheet, not only decreases (algebraically) $d\sigma/d\psi'$ but also increases its variation with wing height.

(c) Dihedral increases $d\sigma/d\psi'$.

Further evidence concerning the flap effect is found in table IX, in which it is shown that flap deflection generally causes a significant increase in stability. Part of the flap effect, however, probably exists at the wing itself; in the tests reported in reference 8, in which the yaw characteristics of wings alone were measured, it was found that deflecting the flaps increased the directional stability of the wings themselves by values between -0.0001 and -0.0003.

Figure 15 shows that, in general, only slight variation in stability occurs with angle of attack. The small observed variations are, in most of the examples, in such a direction as to support the sidewash theory previously given. The large variations are probably due to various

interferences peculiar to each design. Thus, the stability of the low-wing airplanes increases with angle of attack and the stability of high-wing airplanes or flying boats decreases.

STABILITY OF WING-FUSELAGE COMBINATION

Stability of fuselages and hulls.- Data on the directional stability of fuselages and hulls were obtained from results of tests made in the NACA 7- by 10-foot wind tunnel, at the Washington Navy Yard, and at the Russian Central Aero-Hydrodynamical Institute (reference 11).

The stability criterion is chosen as $dC_{n_f}'/d\psi'$, where $C_{n_f}' = N_f'/q$ (vol), in which N_f' is the yawing moment about the reference axis, chosen at 0.3L from the nose. Experimental values of $dC_{n_f}'/d\psi'$ for 5 flying-boat hulls and 12 streamline fuselages are listed in table X together with data on the geometric characteristics of the fuselages and hulls. The flying boat hulls appear to be less unstable than the fuselages.

Theoretical values of $dC_{n_f}'/d\psi'$, as calculated by the methods of reference 12, are also listed in table X for the six fuselages of circular and elliptical cross section. They agree closely with experimental values for three of the fuselages but exceed the experimental values by about 50 percent for the other three. It will be noted that the comparison is not strictly valid, inasmuch as the experimental values, owing to the existence of a resultant cross-wind force, depend on the position of the reference axis. Harrington (reference 10) indicates that this force is confined to the rear leeward surface of the yawed body and is due to the breakdown of the boundary layer in working against an adverse pressure gradient. The recovery of pressure on the rear leeward side of the fuselage does not occur after flow break-down (reference 12), which produces a resultant side force. The magnitude of the yawing moment is therefore dependent not only on the shape parameters of the fuselage that affect the pressure distribution but also on all the other variables that may affect the boundary-layer flow. The yawing moment therefore becomes a function of Reynolds number, roughness, interference, and other related factors.

Fuselage-wing interference.- In general, the sum of the yawing moments of the wing and the fuselage, tested separately, does not equal the yawing moment of the wing-fuselage combination. Data illustrating this difference are given in table XI. Values of the interference factor, defined as

$$F_i = \frac{\left(\frac{dC_n'}{d\psi'}\right)_{f+w}}{\left(\frac{dC_n'}{d\psi'}\right)_f + \left(\frac{dC_n'}{d\psi'}\right)_w}$$

are listed in the last column of the table. The coefficients are based on wing dimensions.

For the two flying boats, the fuselage-wing interference increases the instability. For the fuselages, particularly for that of reference 9, the interference is favorable, reducing the instability of the combination. The effect is greater for the low-wing than for the high-wing combination, the difference being most pronounced for the flap-down condition. In the most favorable case (low wing, flaps down, zero dihedral) the interference was sufficient to make the wing-fuselage combination stable.

The presence of the wing probably increases the intensity of the boundary-layer break-down at the rear leeward side of the fuselage, thereby reducing the instability of the fuselage. Flap deflection magnifies this effect. For flaps up, the experiments indicate that dihedral has no great effect; however, the instability of the fuselage is slightly increased.

APPLICATION TO DESIGN

The foregoing data and methods may be applied to the design of vertical tail surfaces to obtain desired degrees of static directional stability and control. Although the methods are believed essentially sound, the inadequacy of the data somewhat limits their use.

Directional stability.- The directional stability of a proposed design may be conveniently considered in two

parts: that of the wing-fuselage combination, and that of the vertical tail:

$$\left(\frac{dC_n{}'}{d\psi'}\right)_A = \left(\frac{dC_n{}'}{d\psi'}\right)_t + \left(\frac{dC_n{}'}{d\psi'}\right)_{f+w} \tag{6}$$

The fuselage and the wing are usually designed without reference to directional stability, which accordingly depends on the design of the vertical tail.

Contribution of wing and fuselage to stability.- The contribution of the wing and the fuselage may be taken as the value for the most nearly similar wing-fuselage combination of table XI. A somewhat more accurate procedure is to approximate separately the terms of the expression:

$$\left[\left(\frac{dC_n{}'}{d\psi'}\right)_f + \left(\frac{dC_n{}'}{d\psi'}\right)_w\right] F_i$$

The value of $\left(\frac{dC_n{}'}{d\psi'}\right)_f$ may be taken as that for the most nearly similar fuselage of table X multiplied by the ratio of the volume divided by the wing area times the wing span. The value of $\left(\frac{dC_n{}'}{d\psi'}\right)_w$ may be taken as -0.0001 for all unflapped wings, regardless of dihedral, taper ratio, aspect ratio, or sweepback. The interference factor F_i may be taken to be 1.3 for flying-boat hulls or 0.6 for fuselages.

Rudder-fixed stability.- For a desired rudder-fixed stability, the tail may be designed according to equation (4), here rewritten:

$$S_t \frac{dC_{N_t}}{d\alpha_t} = \left(\frac{dC_n{}'}{d\psi'}\right)_t \frac{b_w S_w}{l \frac{q}{q_o}\left(1 - \frac{d\sigma}{d\psi'}\right)}$$

in which

$\left(\frac{dC_n{}'}{d\psi'}\right)_t$ is the difference between the desired stability of the airplane and the stability of the wing-fuselage combination.

S_w, l, b_w are characteristics of the airplane

q/q_o is 0.90 for single tails and 1.00 for twin tails.

$\frac{d\sigma}{d\psi'}$ is assumed equal to the value for the most nearly similar case in table VIII

From the value of $S_t \frac{dC_{N_t}}{d\alpha_t}$ thus calculated, the size and shape of the vertical tail are determined by the use of figure 2 and various practical considerations of the type discussed in reference 13. It must be noted, in the use of figure 3, that the effective aspect ratio of the usual single tail is obtained by multiplying the actual aspect ratio by 1.55.

If wind-tunnel tests of a model have shown unsatisfactory directional characteristics, the procedure just described may be applied, with some modifications to the redesign of the vertical tail. If results were obtained for the model with the tail both attached and removed, $\left(\frac{dC_n'}{d\psi'}\right)_t$ is obtained as the difference between the stabilities for the two conditions, and $\frac{q}{q_o}\left(1 - \frac{d\sigma}{d\psi'}\right)$ can then be obtained directly from equation (4). The design of the new tail, to give the desired stability, then proceeds as before. If tail-removed tests have not been made, it becomes necessary to estimate $\frac{d\sigma}{d\psi'}$ by comparison with a similar airplane in table VIII and then to compute $\left(\frac{dC_n'}{d\psi'}\right)_t$ from equation (4). Subtracting this value from the experimental value of $\left(\frac{dC_n'}{d\psi'}\right)_A$ gives a value for the tail-removed condition, and the tail is then redesigned as before.

Rubber-free stability.- With the rudder free at any angle of yaw, the rudder floats at the angle for which the

hinge moment is zero. This angle may be found by equating (1) to zero and substituting

$$C_{N_t} = \alpha_t \left(\frac{dC_{N_t}}{d\alpha_t}\right) + \tau\,\delta_r \left(\frac{dC_{N_t}}{d\alpha_t}\right)$$

giving

$$\delta_r = -\frac{u\,\dfrac{dC_{N_t}}{d\alpha_t}}{u\,\tau\,\dfrac{dC_{N_t}}{d\alpha_t} + v}\,\alpha_t$$

The normal-force coefficient then becomes

$$C_{N_t} = \left[\frac{v}{u\tau\,\dfrac{dC_{N_t}}{d\alpha_t} + v}\right]\frac{dC_{N_t}}{d\alpha_t}\,\alpha_t$$

The yawing moment due to the tail is then

$$C_{n_t}' = \frac{S_t}{S_w}\,\frac{l}{b_w}\,\frac{q}{q_o}\left[\frac{v}{u\tau\,\dfrac{dC_{N_t}}{d\alpha_t} + v}\right]\frac{dC_{N_t}}{d\alpha_t}\,\alpha_t$$

Finally, the contribution of the vertical tail to the directional stability is

$$\left(\frac{dC_n'}{d\psi'}\right)_t = \frac{S_t}{S_w}\,\frac{l}{b_w}\,\frac{q}{q_o}\left[\frac{v}{u\tau\,\dfrac{dC_{N_t}}{d\alpha_t} + v}\right]\frac{dC_{N_t}}{d\alpha_t}\left(1 - \frac{d\sigma}{d\psi'}\right)$$

This expression is the same as that derived for rudder-fixed stability except for the factor $\left[\dfrac{v}{u\tau\,\dfrac{dC_{N_t}}{d\alpha_t} + v}\right]$.

For any specific design, values of u and v are taken from figures 5 and 6.

Calculations for an average tail indicate that the contribution of the vertical tail, with rudder free, may be reduced to 65 percent of its value with rudder fixed. This value is large enough in somce cases to make the airplane directionally unstable.

Directional control.- A common criterion for directional control is the value of $d\psi'/d\delta_r$. The rudder area corresponding to a given value of this ratio may be found from the equation

$$\tau = \frac{\dfrac{d\psi'}{d\delta_r} \left(\dfrac{dC_n'}{d\psi'}\right)_A}{\dfrac{dC_n'}{d\alpha_t} \dfrac{S_t}{S_w} \dfrac{l}{b_w} \dfrac{q}{q_o}} \tag{7}$$

The value of τ is found from equation (7) and is finally applied to the curves of figure 4 to obtain suitable values of S_r/S_t and S_b/S_r.

Example.- Model 20 is identical with model 19 except that it has a larger vertical tail. It should therefore be possible to calculate the stability of model 20 from that of model 19 and, by a comparison of the calculated with the experimental value, to obtain an indication of the accuracy of the methods just presented.

The value of $\dfrac{d\sigma}{d\psi'}$ is estimated, by reference to table VIII, as 0.15. Then by the application of equation (4), the tail contribution to stability is calculated for model 19:

$$\left(\frac{dC_n'}{d\psi'}\right)_{t_{19}} = -0.020 \times \frac{0.0619}{0.8952} \times \frac{1.141}{2.150} \times 0.85 \times 0.90$$

$$= -0.00056$$

The value of $\dfrac{dC_n'}{d\psi'}$ for the complete model was -0.00054; the contribution of the wing and fuselage $\left(\dfrac{dC_n'}{d\psi'}\right)_{f+w}$ is then -0.00054 + 0.00056 = 0.00002.

For the tail contribution of model 20,

$$\left(\frac{dC_n'}{d\psi'}\right)_{t_{20}} = -0.035 \times \frac{0.1087}{0.8952} \times \frac{1.141}{2.150} \times 0.85 \times 0.90$$

$$= -0.00172$$

The calculated value of $\frac{dC_n'}{d\psi'}$ for model 20 is thus $-0.00172 + 0.00002 = -0.00170$, in fair agreement with the experimental value of -0.00156.

CONCLUSIONS

The more important of the points mentioned in the paper are listed here. Since the data were limited and unsystematic, the conclusions are, to a considerable degree, tentative.

1. The end-plate effect of the horizontal tail increases the effective aspect ratio of a single vertical tail by about 50 percent.

2. The ratio of dynamic pressure at the tail to free-stream dynamic pressure is about 0.90 for single tails and about 1.00 for twin tails not in large nacelle wakes.

3. The induced flow associated with the trailing vortex system of the fuselage and the wing is an important factor in directional stability. The sidewash is favorable for low-wing airplanes and adverse for high-wing airplanes.

4. Flap deflection increases stability, particularly for low-wing airplanes.

5. Dihedral reduces stability, particularly for low-wing airplanes.

6. Flying-boat hulls are generally somewhat less unstable than fuselages. The flying boats tested, however, had unfavorable wing-fuselage interference, generally requiring more vertical tail area than fuselages on aircraft of comparable size.

Langley Memorial Aeronautical Laboratory,
National Advisory Committee for Aeronautics,
Langley Field, Va., July 3, 1940.

REFERENCES

1. Silverstein, Abe, and Katzoff, S.: Aerodynamic Characteristics of Horizontal Tail Surfaces. Rep. No. 688, NACA, 1940.

2. Katzoff, S.: Longitudinal Stability and Control with Special Reference to Slipstream Effects. Rep. No. 690, NACA, 1940.

3. Zimmerman, C. H.: Characteristics of Clark Y Airfoils of Small Aspect Ratios. Rep. No. 431, NACA, 1932.

4. Goett, Harry, J., and Reeder, J. P.: Effects of Elevator Nose Shape, Gap, Balance, and Tabs on the Aerodynamic Characteristics of a Horizontal Tail Surface. Rep. No. 675, NACA, 1939.

5. Glauert, H.: Theoretical Relationships for an Aerofoil with Hinged Flap. R. & M. No. 1095, British A.R.C., 1927.

6. Martinov, A., and Kolosov, E.: Some Data on the Static Longitudinal Stability and Control of Airplanes (Design of Control Surfaces). T.M. No. 941, NACA, 1940.

7. Silverstein, Abe.: Toward a Rational Method of Tailplane Design. Jour. Aero. Sci., vol. 6, no. 9, July 1939, pp. 361-369.

8. Bamber, M. J., and House, R. O.: Wind-Tunnel Investigation of Effect of Yaw on Lateral-Stability Characteristics. I - Four N.A.C.A. 23012 Wings of Various Plan Forms with and without Dihedral. T.N. No. 703, NACA, 1939.

9. Bamber, M. J., and House, R. O.: Wind-Tunnel Investigation of Effect of Yaw on Lateral-Stability Characteristics. II - Rectangular N.A.C.A. 23012 Wing with a Circular Fuselage and a Fin. T.N. No. 730, NACA, 1939.

10. Harrington, R. P.: An Attack on the Origin of Lift of an Elongated Body. Publication No. 2, The Daniel Guggenheim Airship Inst., 1935, pp. 32-52.

11. Imlay, Frederick H.: The Estimation of the Rate of Change of Yawing Moment with Sideslip. T.N. No. 636, NACA, 1938.

12. Upson, Ralph H., and Klikoff, W. A.: Application of Practical Hydrodynamics to Airship Design. Rep. No. 405, NACA, 1931.

13. Root, L. E.: Empennage Design with Single and Multiple Vertical Surfaces. Jour. Aero. Sci., vol. 6, no. 9, July 1939, pp. 353-360.

TABLE I.- GEOMETRIC CHARACTERISTICS OF AIRPLANES AND MODELS

Model	Type of vertical tail	V (mph)	S_w (sq ft)	b_w (ft)	l (ft)	S_t (sq ft)	b_t (ft)	S_r (sq ft)	S_b (sq ft)	A_t	$\frac{S_r}{S_t}$	$\frac{S_b}{S_r}$
1	V	59	172.00	37.5	13.8	10.100	3.70	5.000	0.200	1.34	0.49	0.04
2	III	59	172.00	35.0	14.0	11.000	3.50	6.200	1.500	1.11	.56	.24
3	I	59	287.00	40.0	19.4	25.500	4.10	13.500	1.700	1.29	.53	.13
4	II	59	258.00	39.0	17.0	30.800	6.40	13.200	2.500	1.33	.43	.19
5	V	59	177.00	29.4	16.5	13.500	4.00	7.600	.500	1.19	.56	.07
6	IV	59	338.00	45.8	21.6	37.300	6.30	9.000	2.300	1.04	.24	.26
7	II	97	11.60	10.3	3.6	.840	1.10	.360	.050	1.50	.43	.14
8	I	97	16.70	11.8	4.8	1.390	1.00	.510	.120	1.57	.36	.24
9	I	97	13.00	11.9	3.7	.970	.90	.480	.090	1.76	.50	.19
10	IV	97	15.30	12.3	4.5	1.180	1.20	.350	.090	1.22	.30	.26
11	III	80	8.40	7.7	3.6	.660	.79	.380	.110	.94	.57	.29
12	I	80	5.30	6.3	2.8	.300	.46	.110	.030	1.41	.35	.27
13	I	80	5.50	7.4	2.7	.490	.61	.260	.010	1.55	.53	.05
14	III	80	4.60	6.1	2.6	.260	.45	.130	.005	.79	.49	.04
15	II	80	7.40	8.2	3.1	.500	.79	.190	.050	1.25	.38	.25
16	III	80	10.70	7.7	4.0	1.070	.71	.560	.140	.93	.52	.25
17	V	40	1.11	2.8	1.3	.076	.31	.037	.006	1.30	.50	.15
18	V	40	1.73	2.9	1.7	.138	.40	.076	.005	1.17	.55	.07
19	III	40	.90	2.2	1.1	.062	.15	.029	.006	.38	.46	.20
20	III	40	.90	2.2	1.1	.109	.31	.053	.009	.90	.48	.17
21	III	40	.96	2.5	1.1	.109	.31	.053	.009	.90	.48	.17
22	III	40	.90	2.5	1.1	.071	.22	.033	.007	.68	.47	.21
23	IV	40	.90	2.6	1.3	.084	.24	.031	.006	.68	.37	.19
24	V	40	.60	2.1	.9	.062	.25	.033	.007	.97	.53	.21
25	V	40	1.18	2.9	1.2	.096	.28	.052	.005	1.64	.54	.09
26	IV	40	1.00	2.7	1.1	.095	.31	.042	.007	1.02	.44	.16
27	II	40	1.54	3.0	1.3	.159	.43	.057	.010	1.09	.34	.18
28	II	40	1.34	3.6	1.2	.155	.59	.068	0	2.21	.44	0
29	V	40	1.38	3.1	1.5	.111	.38	.061	.006	1.32	.55	.10
30	II	40	1.02	3.0	1.1	.129	.49	.065	.006	1.84	.50	.10
31	II	40	1.58	3.5	1.4	.108	.44	.065	0	1.80	.60	0
32	II	40	1.06	3.0	1.2	.134	.38	.039	.012	1.10	.29	.31

TABLE II

COMPARISON OF CALCULATED AND EXPERIMENTAL RUDDER EFFECTIVENESS

Model	Effective aspect ratio	$\frac{dC_{N_t}}{d\alpha_t}$	τ	$\frac{q}{q_o}$	$\frac{dC_n'}{d\delta_r}$	
					Calculated	Experimental
1	2.08	0.045	0.68	0.90	-0.00060	-0.00060
2	1.72	.040	.84	.90	- .00077	- .00079
3	1.29	.034	.75	1.00	- .00109	- .00096
4	2.06	.044	.68	.90	- .00140	- .00153
5	1.84	.042	.74	.90	- .00120	- .00118
6 Wing position:						
1 (gull)	----	-----	.47	.90	--------	- .00061
4 (parasol)	----	-----	.47	.90	--------	- .00055
7[a]	2.32	.048	.67	.90	- .00073	- .00074
8	1.57	.038	.63	1.00	- .00081	- .00083
9	1.76	.040	.76	1.00	- .00070	- .00072
10	----	-----	.55	.90	--------	- .00049
11	1.46	.036	.87	.90	- .00104	- .00098
12	1.41	.035	[b].76	1.00	- .00067	- .00068
13	1.55	.037	.71	1.00	- .00085	- .00093
14	1.22	.032	.67	.90	- .00046	- .00049
15	1.94	.043	.66	.90	- .00065	- .00062
16	1.44	.036	.82	.90	- .00138	- .00130
17	2.02	.044	.73	.90	- .00089	- .00104
18	1.81	.041	.76	.85	- .00128	- .00119
19	.59	.020	.72	.90	- .00048	- .00054
20	1.40	.035	.74	.90	- .00150	- .00156
21	1.40	.035	.73	.90	- .00119	- .00127
22	1.04	.029	.74	.90	- .00070	- .00078
23	----	-----	.61	.90	--------	- .00075
24	1.50	.037	.81	.90	- .00128	- .00129
25	2.54	.050	.75	.90	- .00113	- .00114
26	----	-----	.58	.90	--------	- .00085
27	1.69	.040	.58	.90	- .00101	- .00108
28	3.42	.058	.61	.90	- .00127	- .00144
29	2.05	.044	.75	.90	- .00112	- .00116
30	1.84	.041	.70	.90	- .00118	- .00119
31	2.79	.053	.75	.90	- .00101	- .00103
32	1.71	.040	.56	.90	- .00098	- .00109

[a]Horizontal-tail spans 2.58 and 3.11 ft were tested.

[b]From 0.66 x 1.15, for sealed gap.

TABLE III

EFFECT OF HORIZONTAL TAIL ON RUDDER EFFECTIVENESS

Model	α (deg)	T_c (a)	$\frac{dC_n'}{d\delta_r}$		Reduction (percent)
			Horizontal tail on	Horizontal tail off	
4	1.3	----	-0.00153	-0.00147	4
	7.8	----	- .00152	- .00145	5
	12.8	----	- .00151	- .00143	5
6 Wing position: 1 (gull)	-1	----	- .00061	- .00064	-5
	4	----	- .00061	- .00065	-7
	9	----	- .00062	- .00065	-5
	14	----	- .00064	- .00065	-2
	-1	0.56	- .00130	- .00138	-6
	4	.56	- .00135	- .00147	-9
	9	.56	- .00142	- .00153	-8
	14	.56	- .00151	- .00161	-7
4 (parasol)	-1	----	- .00055	- .00061	-11
	4	----	- .00055	- .00062	-13
	9	----	- .00058	- .00063	-9
	14	----	- .00058	- .00064	-10
	-1	.55	- .00112	- .00119	-6
	4	.55	- .00121	- .00127	-5
	9	.55	- .00128	- .00137	-7
	14	.55	- .00137	- .00149	-9

[a]Missing values indicate that propeller was removed.

TABLE IV

EFFECT OF WING POSITION ON RUDDER EFFECTIVENESS

AIRPLANE 6

Wing position	T_c (a)	$\frac{dC_n'}{d\delta_r}$			
		α (deg)			
		-1	4	9	14
1 (gull)	----	-0.00061	-0.00061	-0.00062	-0.00064
2	----	- .00059	- .00060	- .00061	- .00061
3	----	- .00057	- .00058	- .00057	- .00058
4	----	- .00055	- .00055	- .00058	- .00058
1 (gull)	0.56	- .00130	- .00135	- .00142	- .00151
2	.55	- .00118	- .00125	- .00133	- .00141
3	.54	- .00119	- .00127	- .00133	- .00141
4	.53	- .00112	- .00121	- .00128	- .00137

[a]Missing values indicate that propeller was removed.

TABLE V

EFFECT OF FLAPS ON RUDDER EFFECTIVENESS

Model	α (deg)		$\frac{dC_n'}{d\delta_r}$	
	Flaps up	Flaps down	Flaps up	Flaps down
1	-0.9	-1.5	-0.00060	-0.00060
	8.3	7.7	- .00060	- .00059
	8.8	8.9	- .00060	- .00060
	13.2	12.7	- .00059	- .00059
2	8.5	12.7	- .00079	- .00052
	17.9	----	- .00052	-------
16	.1	.6	- .00130	- .00128
	11.0	11.5	- .00130	- .00128
22	10.5	10.8	- .00078	- .00078
23	10.0	10.3	- .00075	- .00075
	16.9	15.1	- .00060	- .00025
24	9.9	10.0	- .00129	- .00129
	----	14.8	-------	- .00043
26	11.1	8.5	- .00085	- .00085
29	11.8	10.9	- .00116	- .00113
3	2.7	14.8	- .00096	- .00096
15	-1.8	6.4	- .00062	- .00059
27	0	12.4	- .00108	- .00108
31	.7	5.2	- .00103	- .00103
32	1.1	9.6	- .00109	- .00095

TABLE VI

COMPARISON OF RUDDER EFFECTIVENESS BASED ON

TWO METHODS OF DEFINING RUDDER AREA

TYPE III TAILS

Model	$\frac{\left(\frac{dC_n'}{d\delta_r}\right)_{above}}{\left(\frac{dC_n'}{d\delta_r}\right)_{exp}}$	$\frac{\left(\frac{dC_n'}{d\delta_r}\right)_{total}}{\left(\frac{dC_n'}{d\delta_r}\right)_{exp}}$
2	0.90	0.98
11	.95	1.06
14	.78	.94
19	.63	.89
20	.79	.96
21	.78	.94
22	.67	.90
24	.84	.99

TABLE VII

EFFECT OF PROPELLER OPERATION ON RUDDER EFFECTIVENESS

Model	ψ' (deg)	α (deg)	T_c (a)	$\frac{dC_n'}{d\delta_r}$
1	0	8.8	----	-0.00060
	0	8.8	[b]0.36	- .00060
	5	8.8	----	- .00061
	5	8.8	[b].36	- .00060
	10	8.8	----	- .00064
	10	8.8	[b].36	- .00069
2	0	- .7	----	- .00079
	0	- .7	.58	- .00078
	0	8.5	----	- .00079
	0	8.3	.64	- .00079
	0	17.9	----	- .00052
	0	15.7	[c].71	- .00054
3	0	14.8	----	- .00096
	0	13.9	.28	- .00120
4	0	1.3	----	- .00153
	0	1.3	.05	- .00159
	0	7.8	----	- .00152
	0	7.7	.26	- .00243
	0	12.7	----	- .00151
	0	12.4	.59	- .00307
6 Wing position: 1 (gull)	0	-1	----	- .00061
	0	-1	.56	- .00130
	0	4	----	- .00061
	0	4	.56	- .00135
	0	9	----	- .00062
	0	9	.56	- .00142
	0	14	----	- .00064
	0	14	.56	- .00151
4 (parasol)	0	-1	----	- .00055
	0	-1	.55	- .00112
	0	4	----	- .00055
	0	4	.55	- .00121
	0	9	----	- .00058
	0	9	.55	- .00128
	0	14	----	- .00058
	0	14	.55	- .00137

[a]Missing values indicate that propeller was removed.
[b]Right-hand propellers only operating.
[c]Single-engine operation, left propeller only operating.

TABLE VIII.- DIRECTIONAL STABILITY AND ESTIMATION OF SIDEWASH

Model	α (deg)	δ_f (deg)	Dihedral (deg)	Wing position (relative to fuselage)	$dC_n'/d\psi'$				Estimated $\frac{d\sigma}{d\psi'}$
					Complete model	Complete model less vertical tail	Effect of vertical tail	Calculated effect of vertical tail $\left(\frac{d\sigma}{d\psi'}=0\right)$	
1	-1.0	0	5.3	Middle	-0.00092	-0.00003	-0.00089	-0.00088	-0.01
7	5.0	0	3.0	High	- .00086	.00030	- .00116	- .00108	- .07
8	- .3	0	3.5	Low	- .00074	.00003	- .00077	- .00128	.40
11	0	0	2.7	Low	- .00075	.00007	- .00082	- .00120	.32
12[a]	-4.0	0	3.0	High	- .00013	.00048	- .00061	- .00089	.31
13	2.3	0	3.0	High	- .00014	.00085	- .00099	- .00120	.18
27	2.2	0	2.4	Low	- .00150	.00025	- .00175	- .00175	0
From reference 9					Fuselage + wing + vertical tail	Fuselage + wing			
	5	0	0	High	- .00080	.00035	- .00115	- .00199	.42
	5	0	0	Middle	- .00107	.00041	- .00148	- .00199	.26
	5	0	0	Low	- .00152	.00030	- .00182	- .00199	.09
	0	60	0	High	- .00120	.00030	- .00150	- .00199	.25
	0	60	0	Middle	- .00150	.00020	- .00170	- .00199	.15
	0	60	0	Low	- .00267	- .00010	- .00257	- .00199	- .29
	5	0	5	High	- .00038	.00037	- .00075	- .00199	.62
	5	0	5	Middle	- .00093	.00041	- .00134	- .00199	.33
	5	0	5	Low	- .00123	.00035	- .00158	- .00199	.21
	0	60	5	High	- .00070	.00040	- .00110	- .00199	.45
	0	60	5	Middle	- .00120	.00030	- .00150	- .00199	.25
	0	60	5	Low	- .00190	.00010	- .00200	- .00199	- .01

[a]Blisters and cockpit enclosure removed.

TABLE IX

EFFECT OF FLAPS ON DIRECTIONAL STABILITY OF COMPLETE AIRPLANE

Model	α (deg)		$\frac{dC_n'}{d\psi'}$	
	Flaps up	Flaps down	Flaps up	Flaps down
1	-1.0	----	-0.00092	--------
	[a]10.1	[a]8.8	- .00124	-0.00147
7	8.5	8.5	- .00075	- .00069
8	9.5	8.0	- .00045	- .00093
12	-4.1	[a]-3.9	- .00022	- .00028
	2.2	[a]2.4	- .00028	- .00025
	8.4	[a]8.7	- .00038	- .00015
13	2.3	[a]2.3	- .00014	- .00023
	[b]2.3	[a,b]2.3	- .00025	- .00020
15	-1.8	[a]6.4	- .00096	- .00115
22	10.5	10.8	- .00095	- .00100
23	10.0	10.3	- .00071	- .00114
	16.9	15.1	- .00071	- .00060
25	10.9	9.3	- .00118	- .00174
26	11.1	8.5	- .00119	- .00133
27	0	12.4	- .00137	- .00182
29	12.5	10.9	- .00121	- .00145
31	.7	[a]5.2	- .00109	- .00120
32	1.1	9.6	- .00137	- .00137

[a]Landing gear extended.
[b]Empennage raised $1\frac{1}{8}$ in.

TABLE X

FUSELAGE AND HULL CHARACTERISTICS

Model	Reference	V (mph)	L (ft)	Projected side area (sq ft)	Volume (cu ft)	$-C_{Y_\beta}$ $\frac{dC_{Y_f}'}{d\psi'}$	$-C_{n_\beta}$ $\frac{dC_{N_f}'}{d\psi'}$ Experimental	Calculated
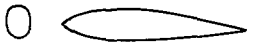	11	40	1.957	0.429	0.0683	0.0034	0.038	0.035
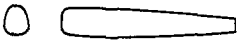	11	40	1.759	.413	.0766	.0063	.021	---
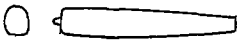	11	40	1.834	.425	.0768	.0084	.023	---
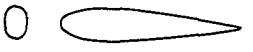	11	40	1.849	.409	.0651	.0072	.031	.034
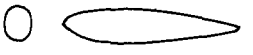	11	40	1.513	.282	.0430	.0032	.024	.025
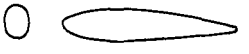	11	40	1.590	.316	.0534	.0066	.022	.031
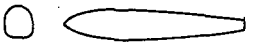	11	40	1.908	.453	.0966	.0049	.025	---
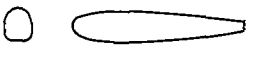	11	40	1.792	.446	.0946	.0043	.026	---
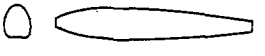	11	40	1.670	.532	.0624	.0064	.028	---
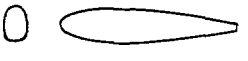	11	78	3.373	1.468	.3780	.0078	.027	---
	11	78	2.625	.832	.1870	.0107	.018	---
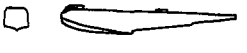	11	78	2.953	.781	.2220	.0094	.019	---
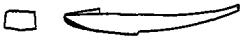	11	78	2.205	.474	.1280	.0095	.011	---
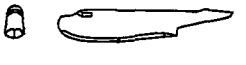	From unpublished results of 7- by 10-foot wind tunnel	80	4.010	3.000	1.0700	.0106	.022	---
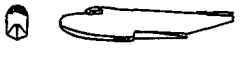		80	4.080	2.285	.7500	.0094	.015	---
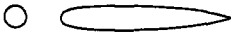		80	4.420	2.180	.8750	.0046	.018	0.027
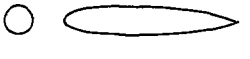	9	80	3.360	1.474	.6100	.0044	.019	.027

TABLE XI. - FUSELAGE-WING INTERFERENCE

Model	α (deg)	δ_{flap} (deg)	Dihedral (deg)	Wing position	$dC_n'/d\psi'$				Fuselage-wing interference factor F_i
					Fuselage or hull alone	Wing alone	Sum	Fuselage or hull + wing	
12	-4	0	3	High	0.00050	-0.00005	0.00045	0.00047	1.04
	11	0	3	-- do --	.00050	- .00008	.00042	.00032	.76
13	2	0	3	-- do --	.00068	- .00004	.00064	.00085	1.33
14	3	0	4.8	-- do --	.00050	- .00007	.00043	.00100	2.32
	11	0	4.8	-- do --	.00087	- .00015	.00072	.00100	1.39
From reference 9	5	0	0	-- do --	.00060	0	.00060	.00035	.58
	5	0	0	Middle	.00060	0	.00060	.00041	.68
	5	0	0	Low	.00060	0	.00060	.00030	.50
	0	60	0	High	.00060	- .00010	.00050	.00030	.61
	0	60	0	Middle	.00060	- .00010	.00050	.00020	.40
	0	60	0	Low	.00060	- .00010	.00050	- .00010	- .20
	5	0	5	High	.00060	0	.00060	.00037	.62
	5	0	5	Middle	.00060	0	.00060	.00041	.68
	5	0	5	Low	.00060	0	.00060	.00035	.58
	0	60	5	High	.00060	- .00020	.00040	.00040	1.00
	0	60	5	Middle	.00060	- .00020	.00040	.00030	.75
	0	60	5	Low	.00060	- .00020	.00040	.00010	.25

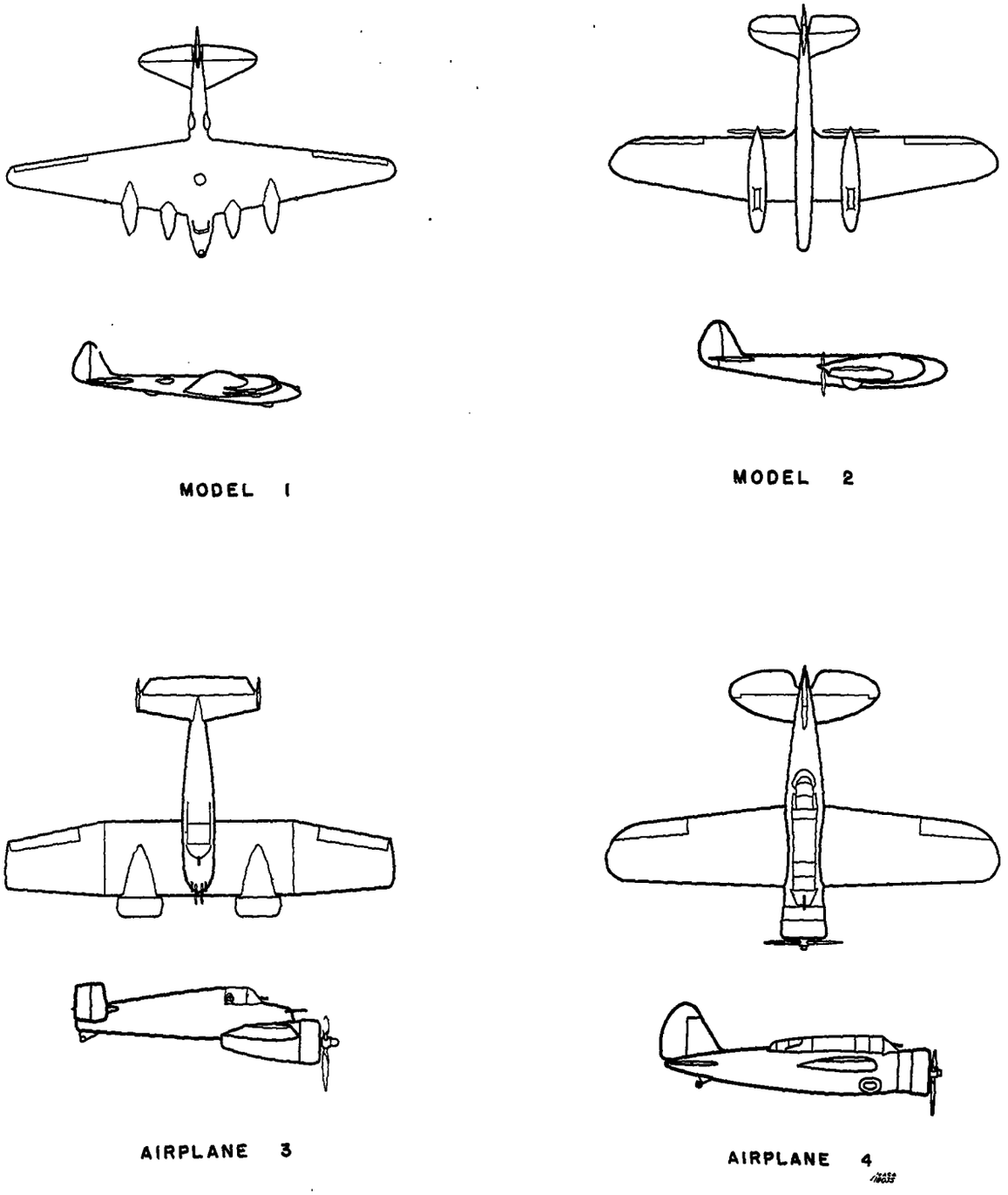

Figure 1(a).- Geometric characteristics of airplanes and models.

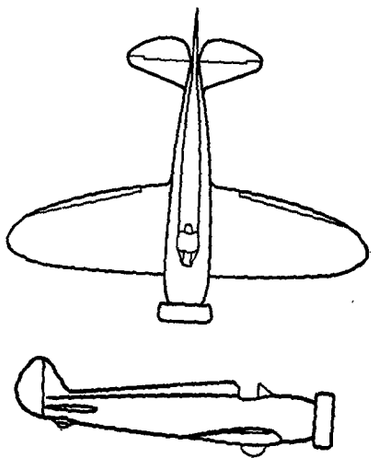

AIRPLANE 5

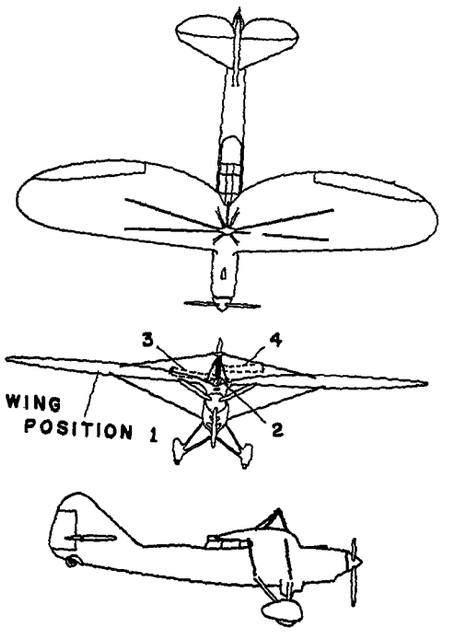

AIRPLANE 6

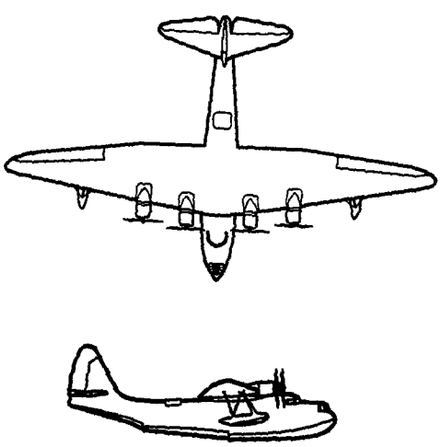

MODEL 7

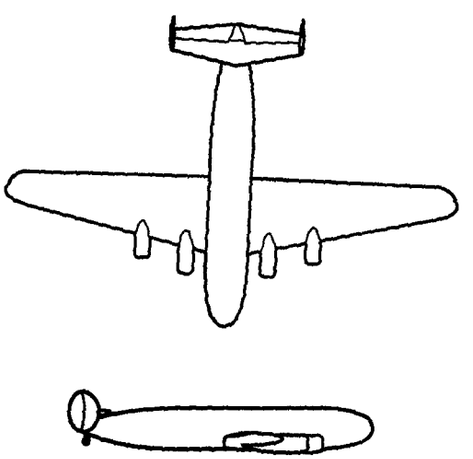

MODEL 8

Figure 1(b). - Geometric characteristics of airplanes and models.

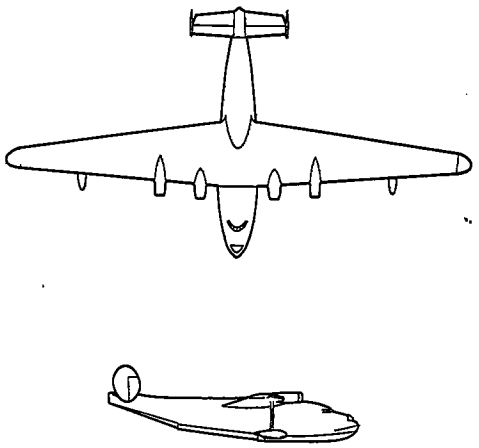

MODEL 9

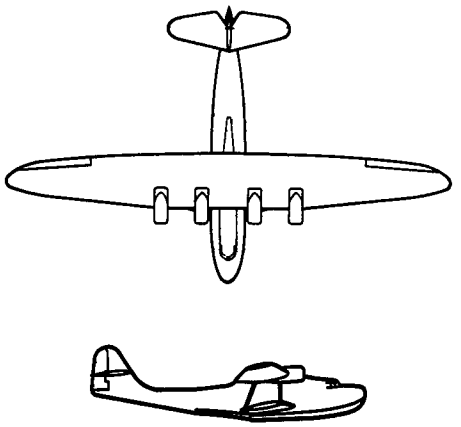

MODEL 10

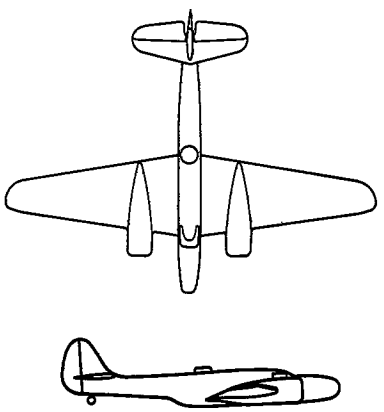

MODEL 11

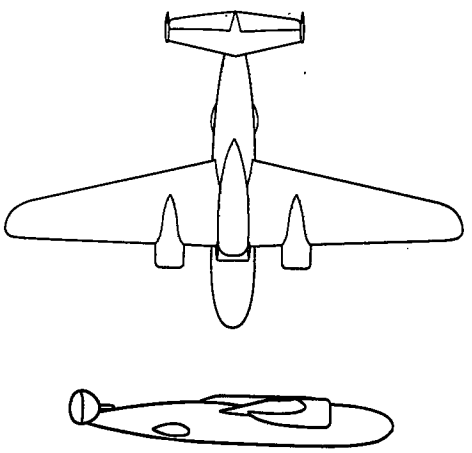

MODEL 12

Figure 1(c). - Geometric characteristics of airplanes and models.

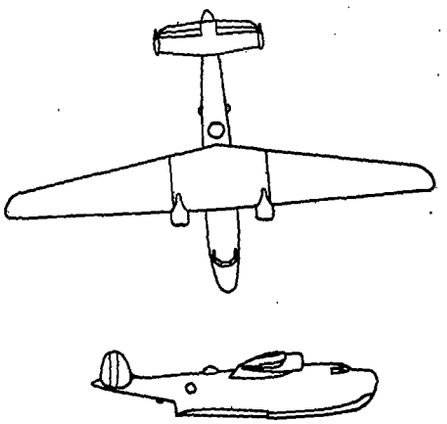

MODEL 13

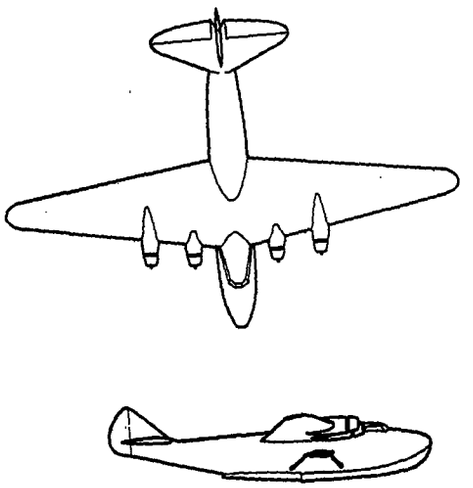

MODEL 14

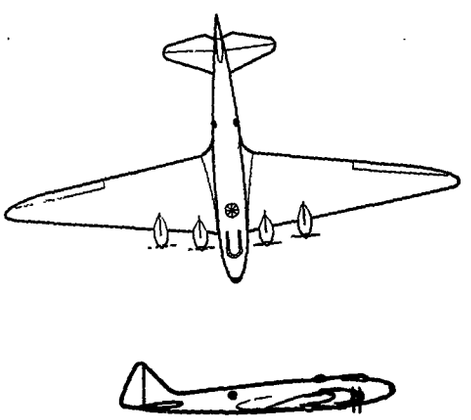

MODEL 15

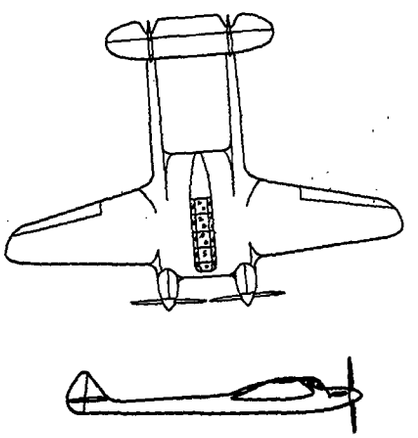

MODEL 16

Figure 1(d). - Geometric characteristics of airplanes and models.

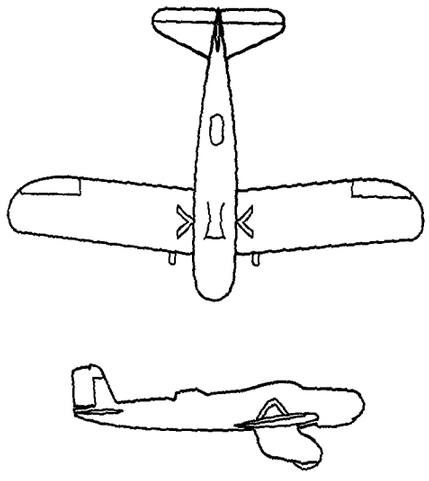

MODEL 17

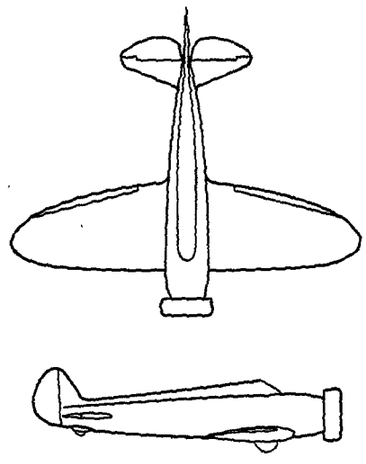

MODEL 18

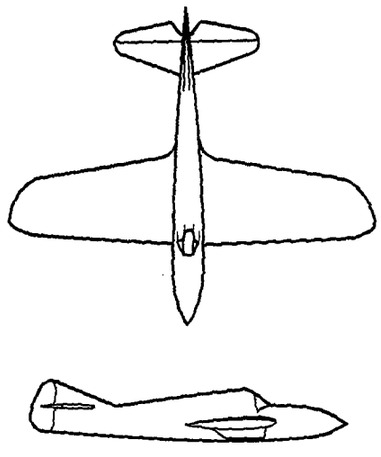

MODEL 19

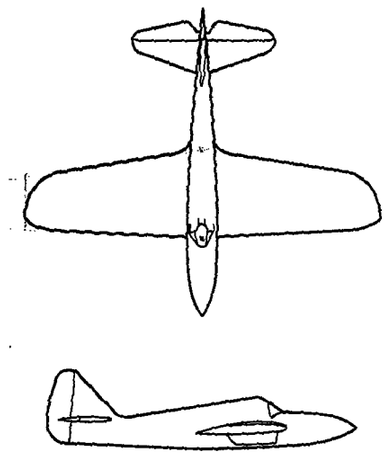

MODEL 20

Figure 1(e). - Geometric characteristics of airplanes and models.

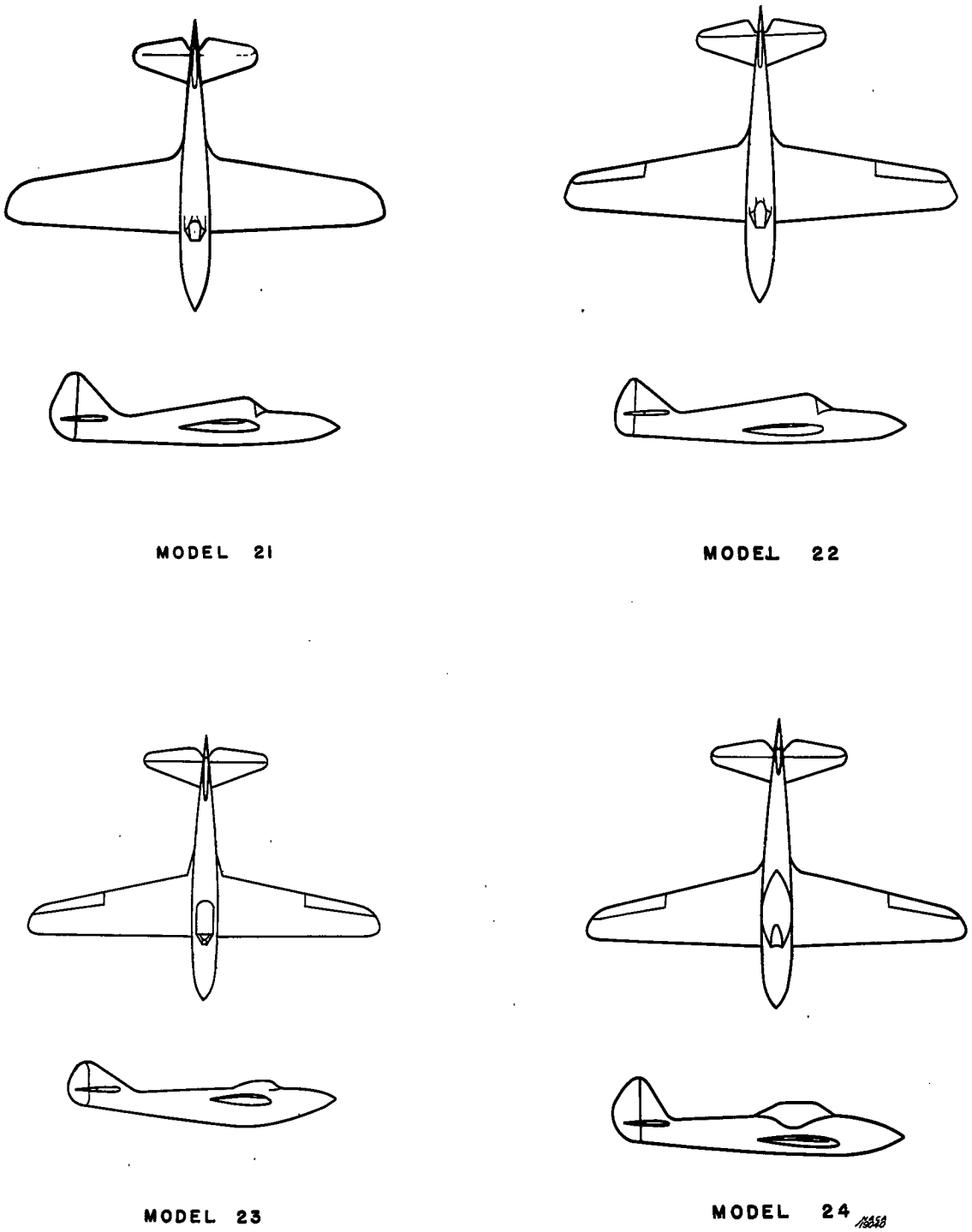

Figure 1(f). - Geometric characteristics of airplanes and models.

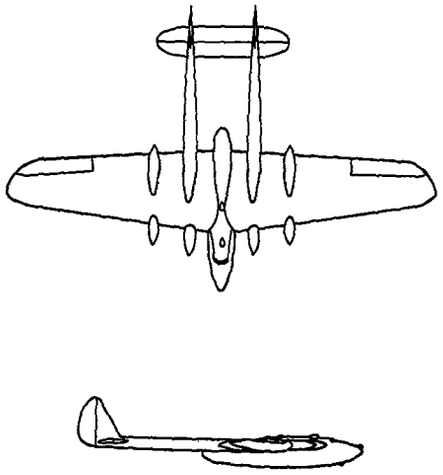

MODEL 25

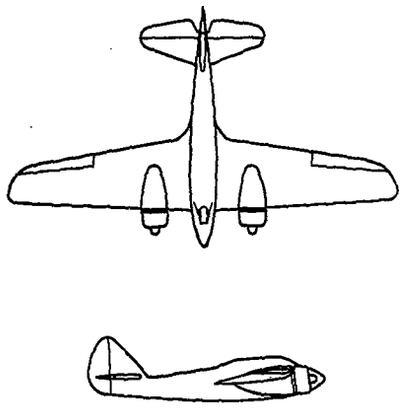

MODEL 26

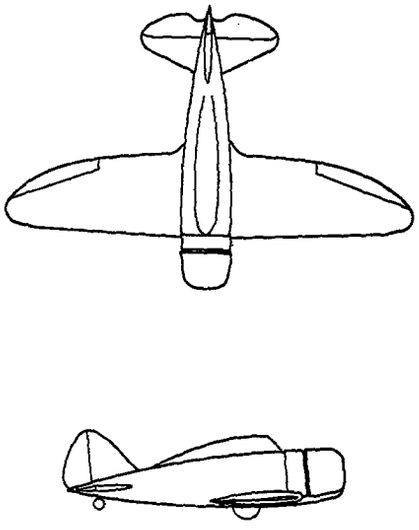

MODEL 27

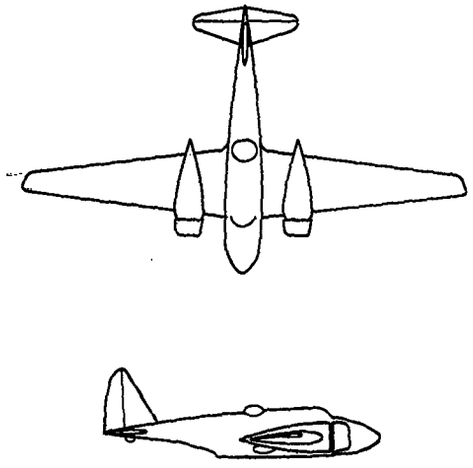

MODEL 28

Figure 1(g). - Geometric characteristics of airplanes and models.

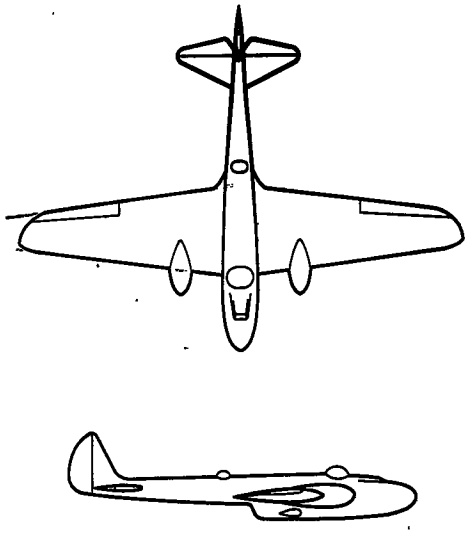

MODEL 29

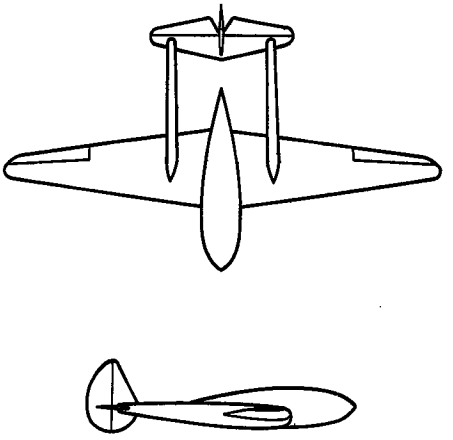

MODEL 30

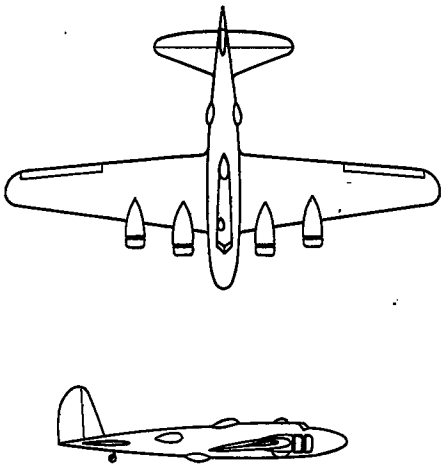

MODEL 31

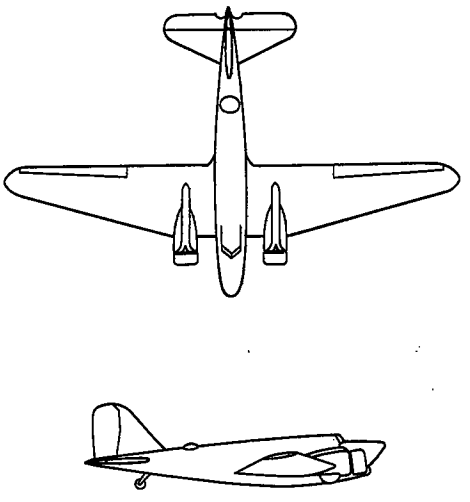

MODEL 32

Figure 1(h). - Geometric characteristics of airplanes and models.

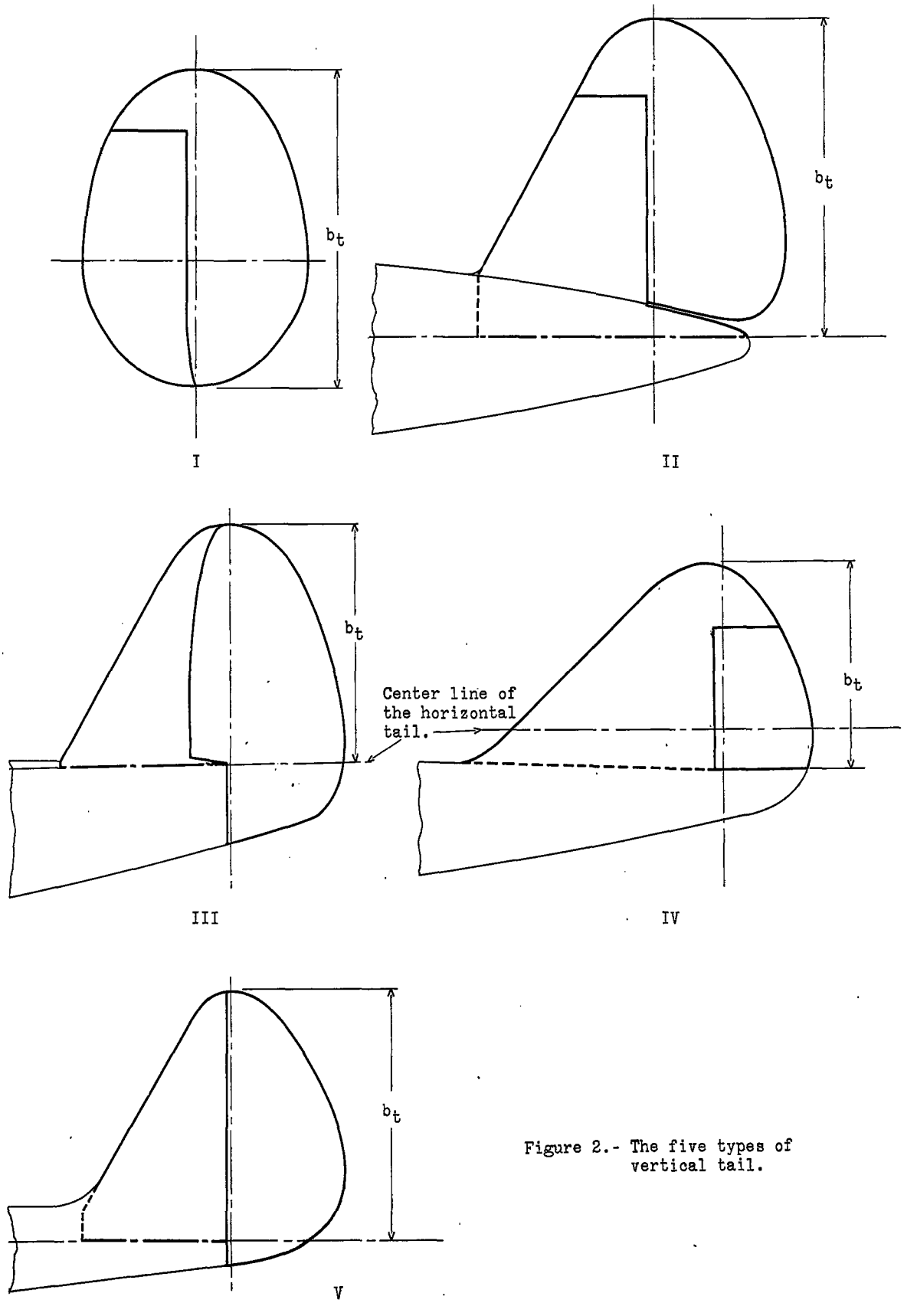

Figure 2.- The five types of vertical tail.

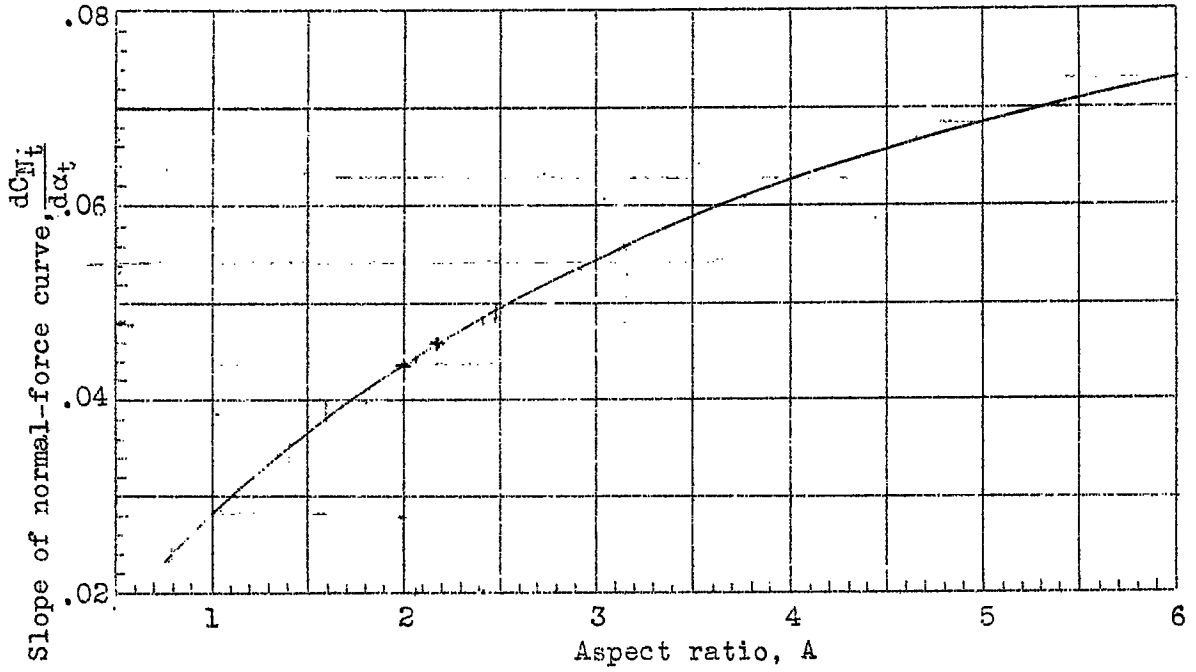

Figure 3.- Variation of slope of the normal-force curve with aspect ratio, A. Results for $A \leqq 3$ from reference 3, results for $A \geqq 3$ from reference 1.

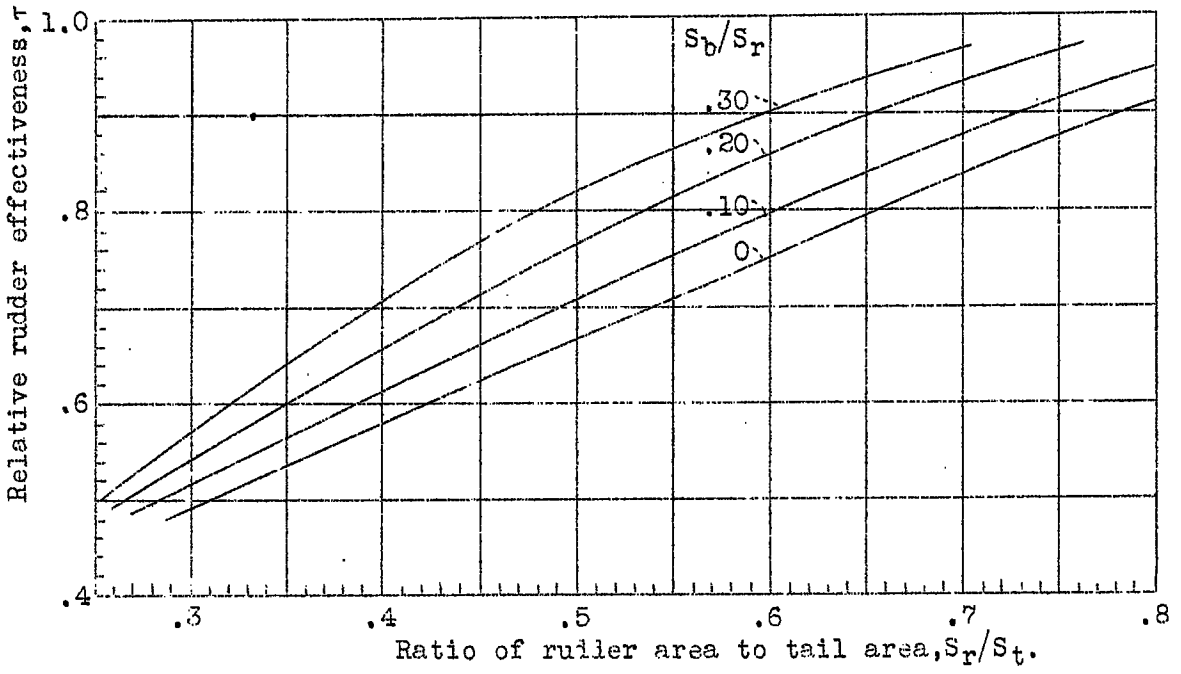

Figure 4.- Variation of relative rudder effectiveness with S_r/S_t and S_b/S_r (from Fig.19 of reference 2).

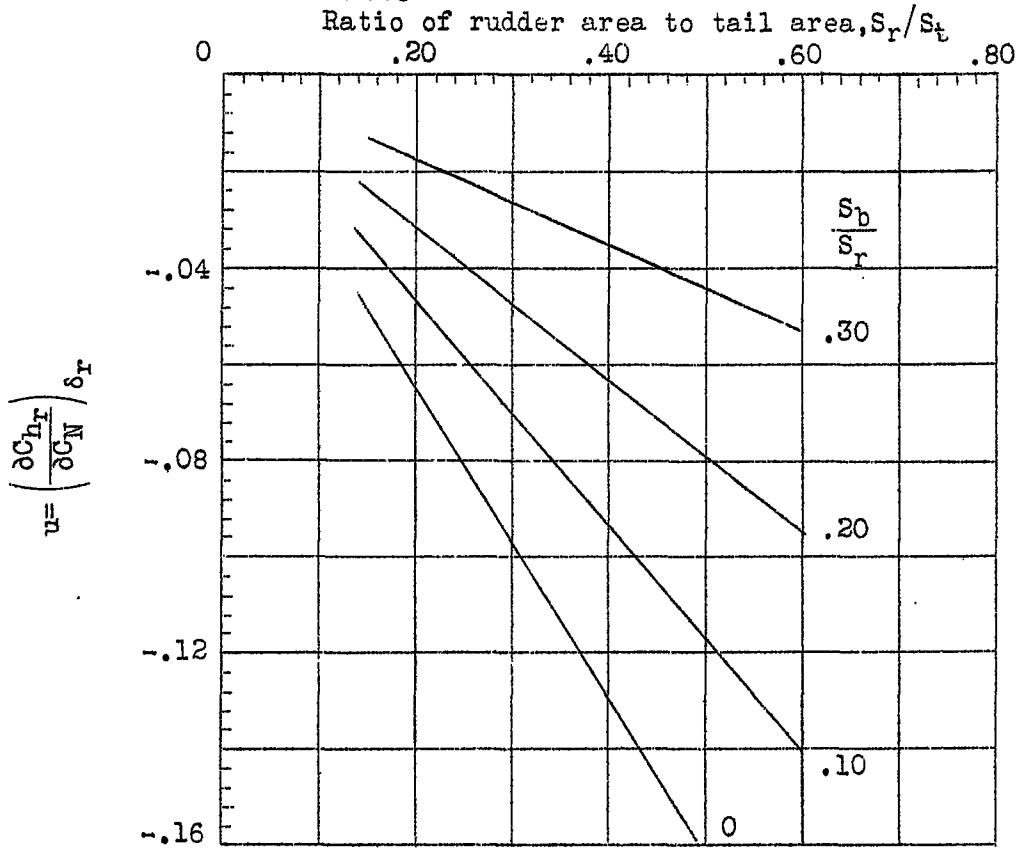

Figure 5.- Variation of the hinge-moment parameter u with $\frac{S_r}{S_t}$ and $\frac{S_b}{S_r}$.

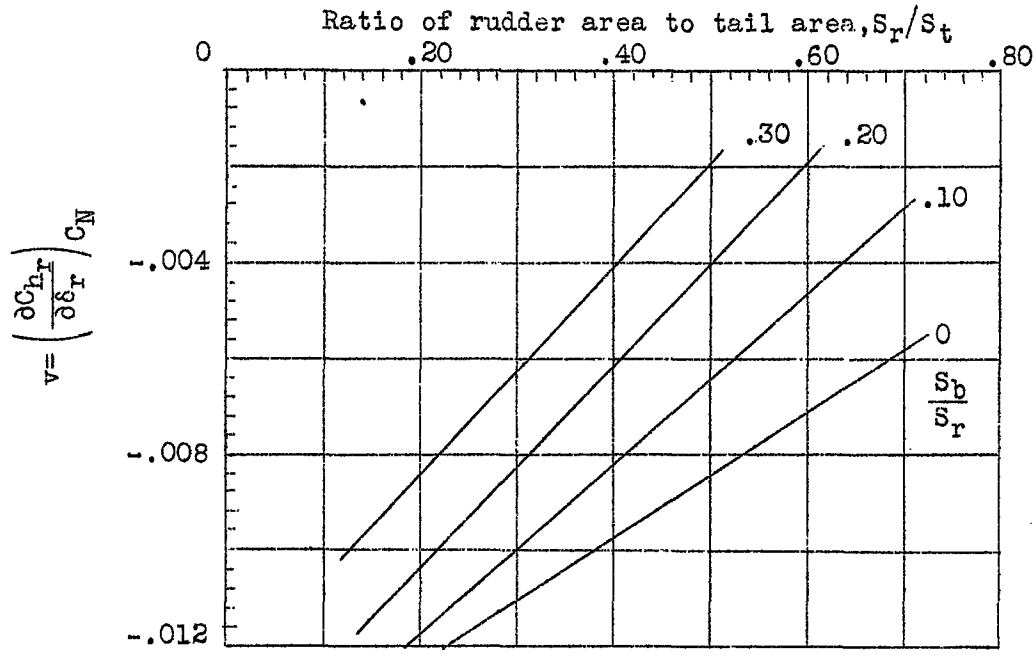

Figure 6.- Variation of the hinge-moment parameter v with $\frac{S_r}{S_t}$ and $\frac{S_b}{S_r}$.

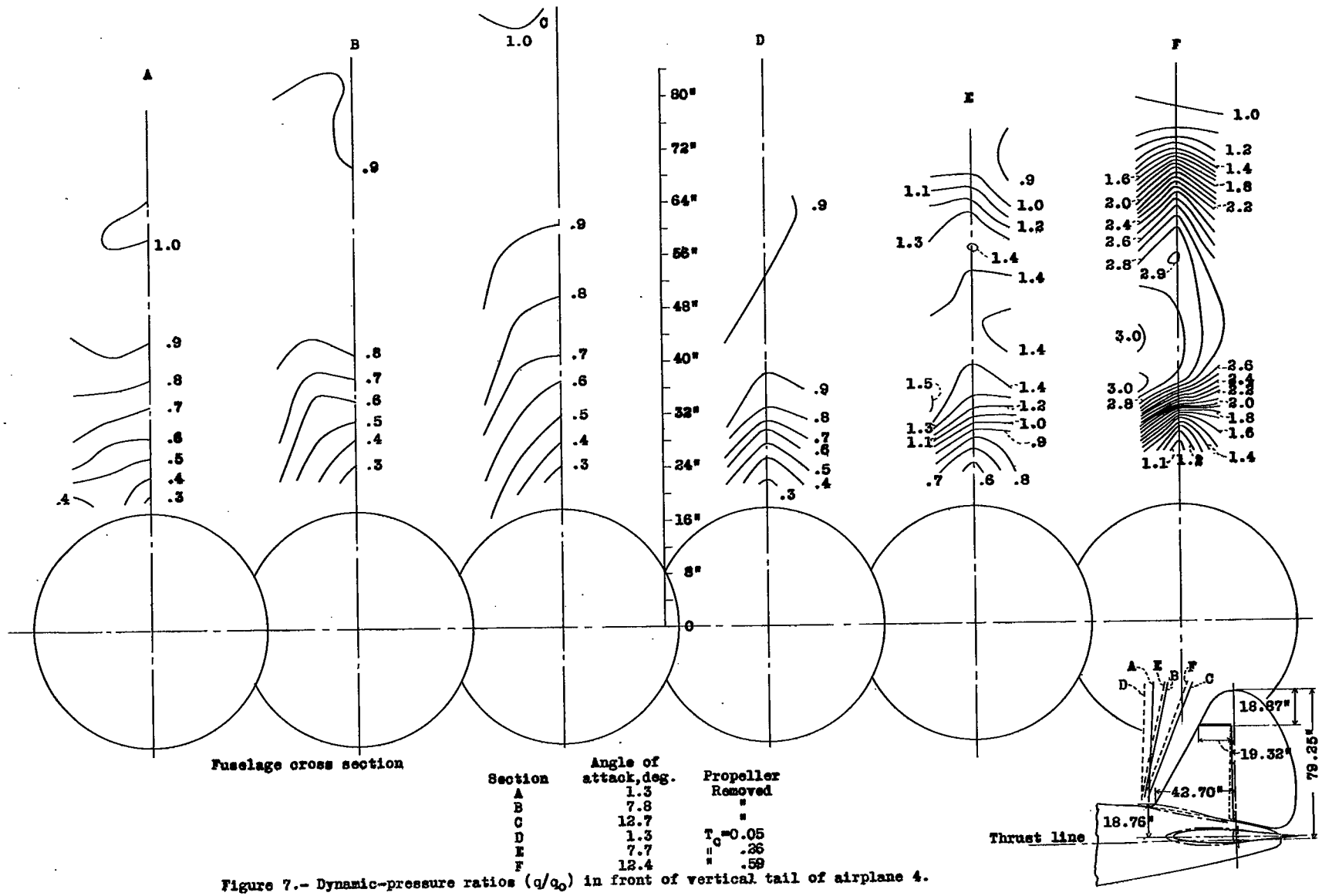

Section	Angle of attack, deg.	Propeller Removed
A	1.3	"
B	7.8	"
C	12.7	"
D	1.3	T_c=0.05
E	7.7	" .26
F	12.4	" .59

Figure 7.- Dynamic-pressure ratios (q/q_o) in front of vertical tail of airplane 4.

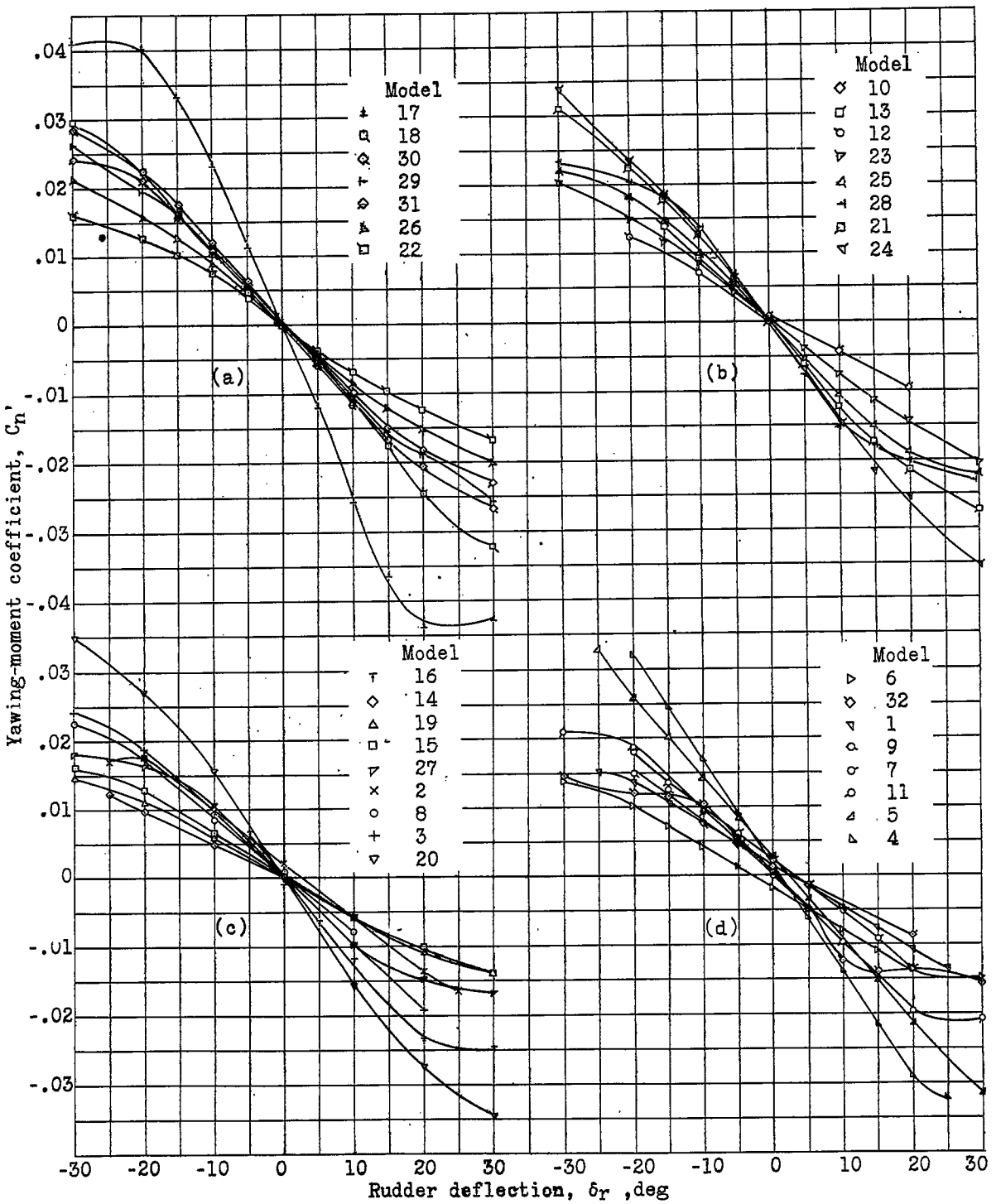

Figure 8.- Variation of yawing-moment coefficient with rudder deflection.

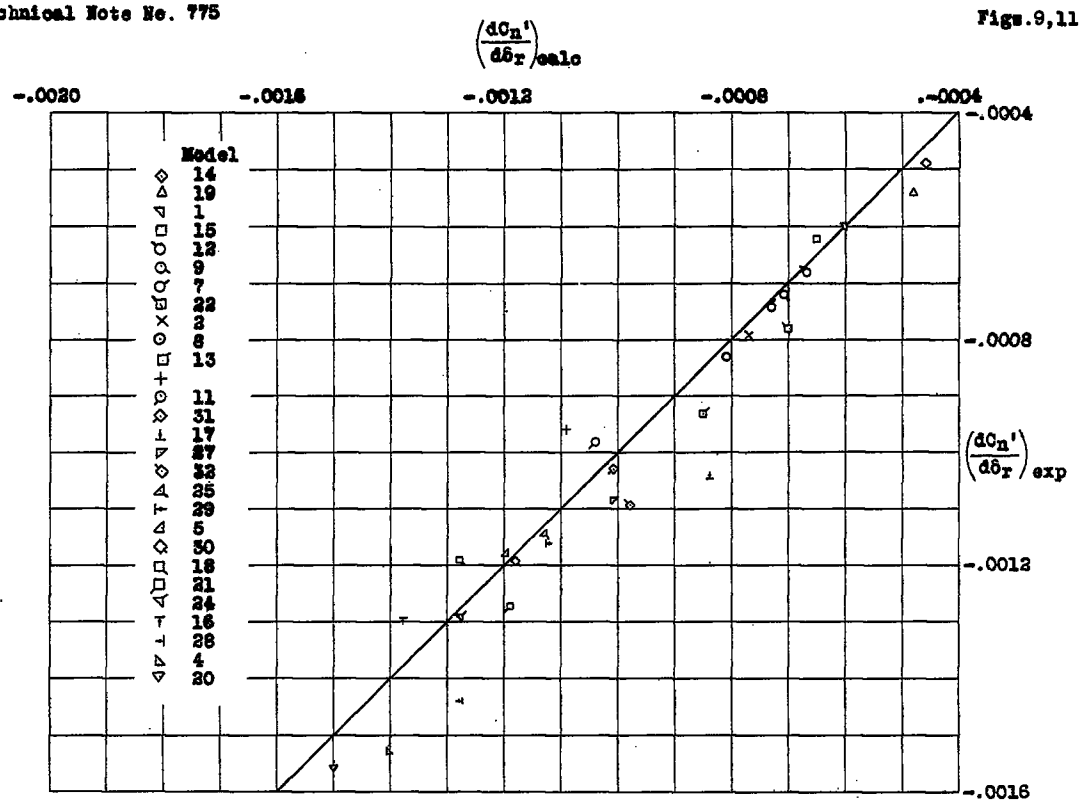

Figure 9.- Comparison between calculated and experimental rudder effectiveness.

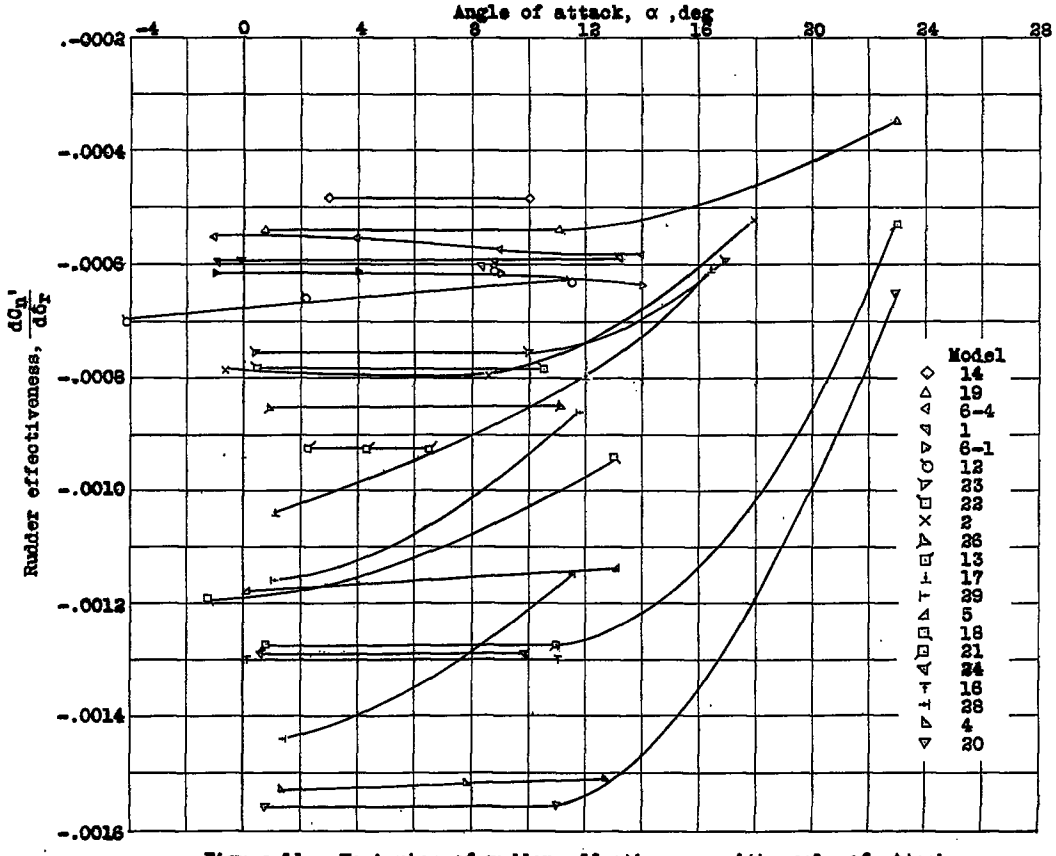

Figure 11.- Variation of rudder effectiveness with angle of attack.

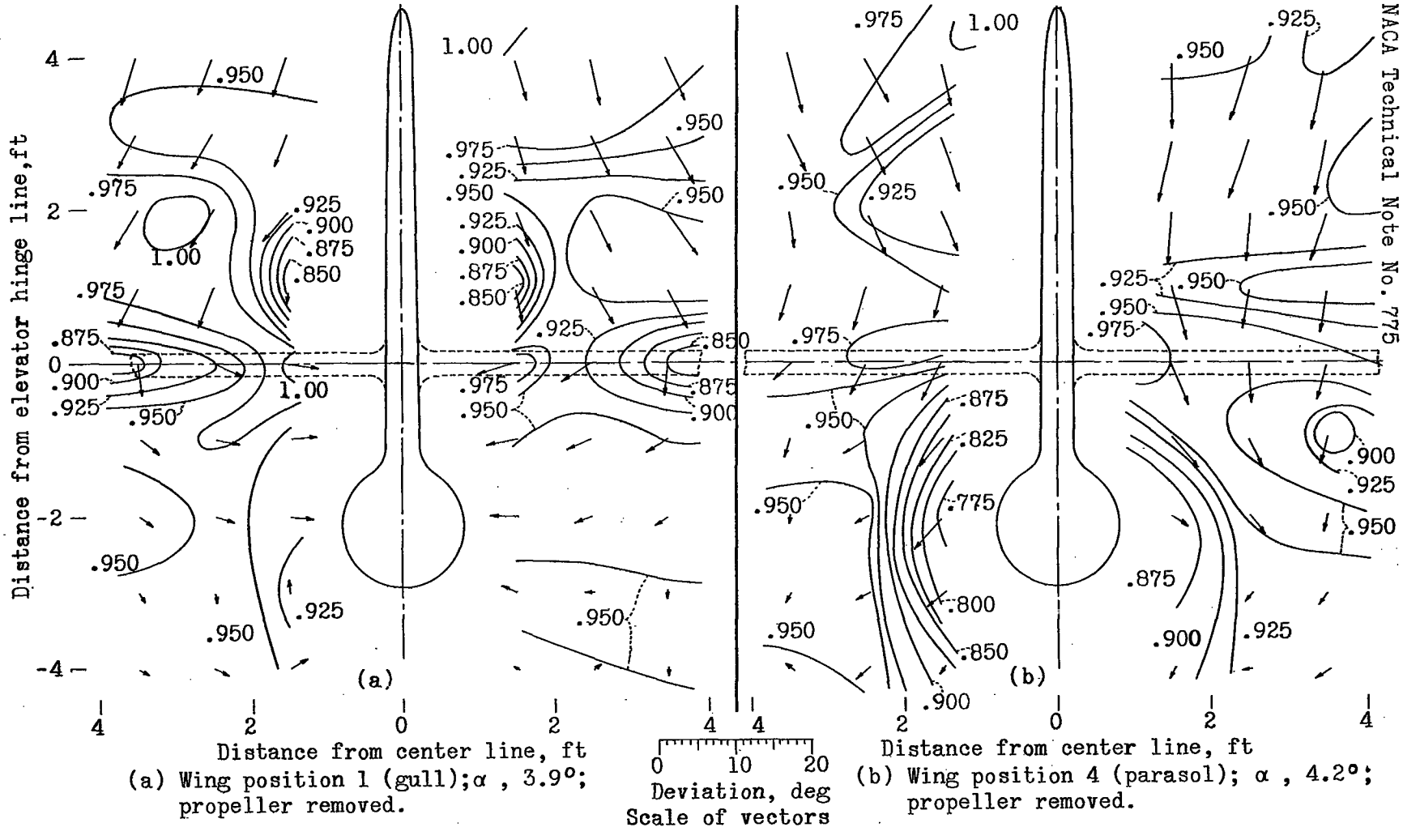

(a) Wing position 1 (gull); α , 3.9°; propeller removed.

(b) Wing position 4 (parasol); α , 4.2°; propeller removed.

Figure 10.- Dynamic-pressure ratios (q/q_o) and downwash angles in plane of elevator hinge line of airplane 6.

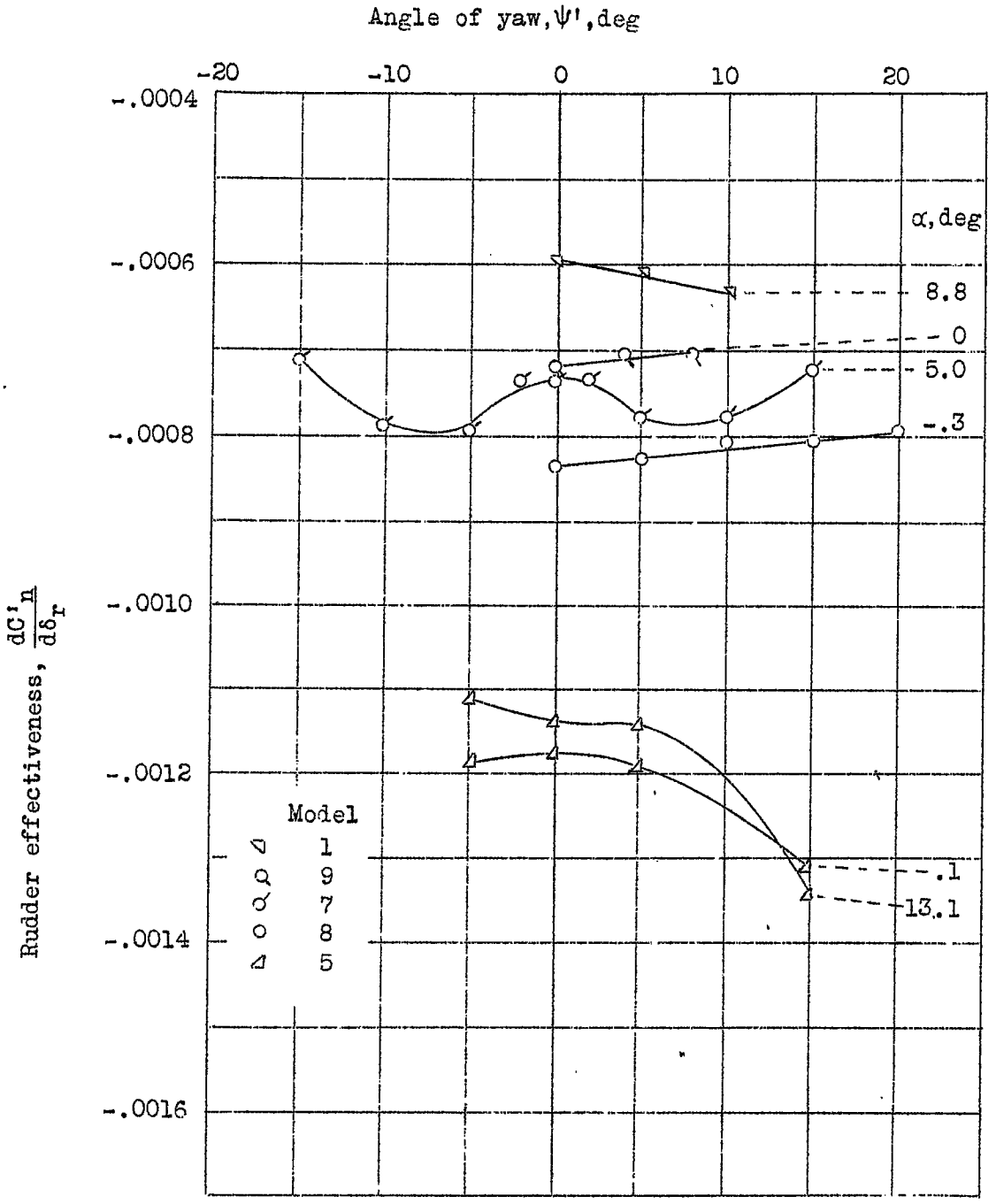

Figure 12.- Variation of rudder effectiveness with angle of yaw.

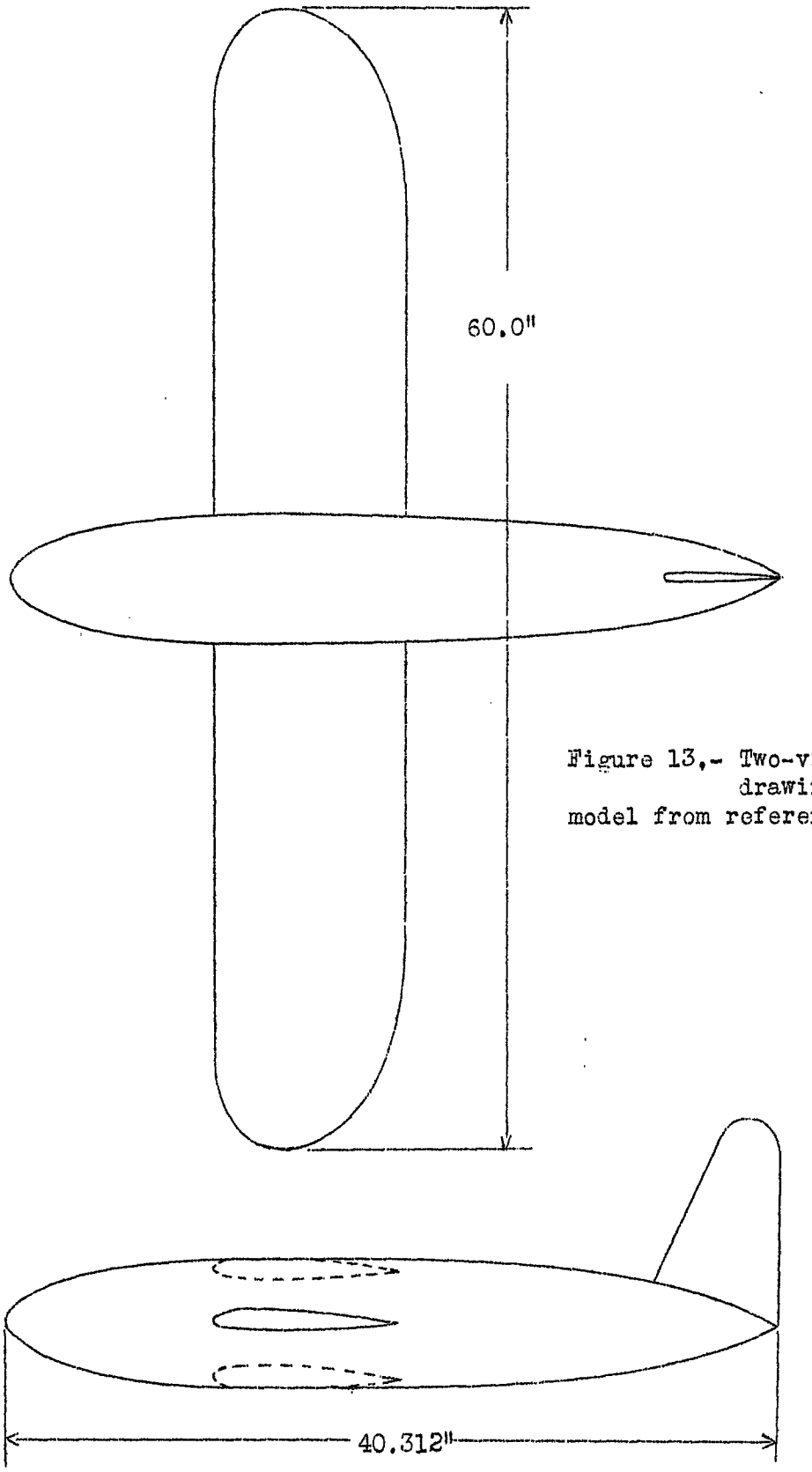

Figure 13.- Two-view drawing of model from reference 9.

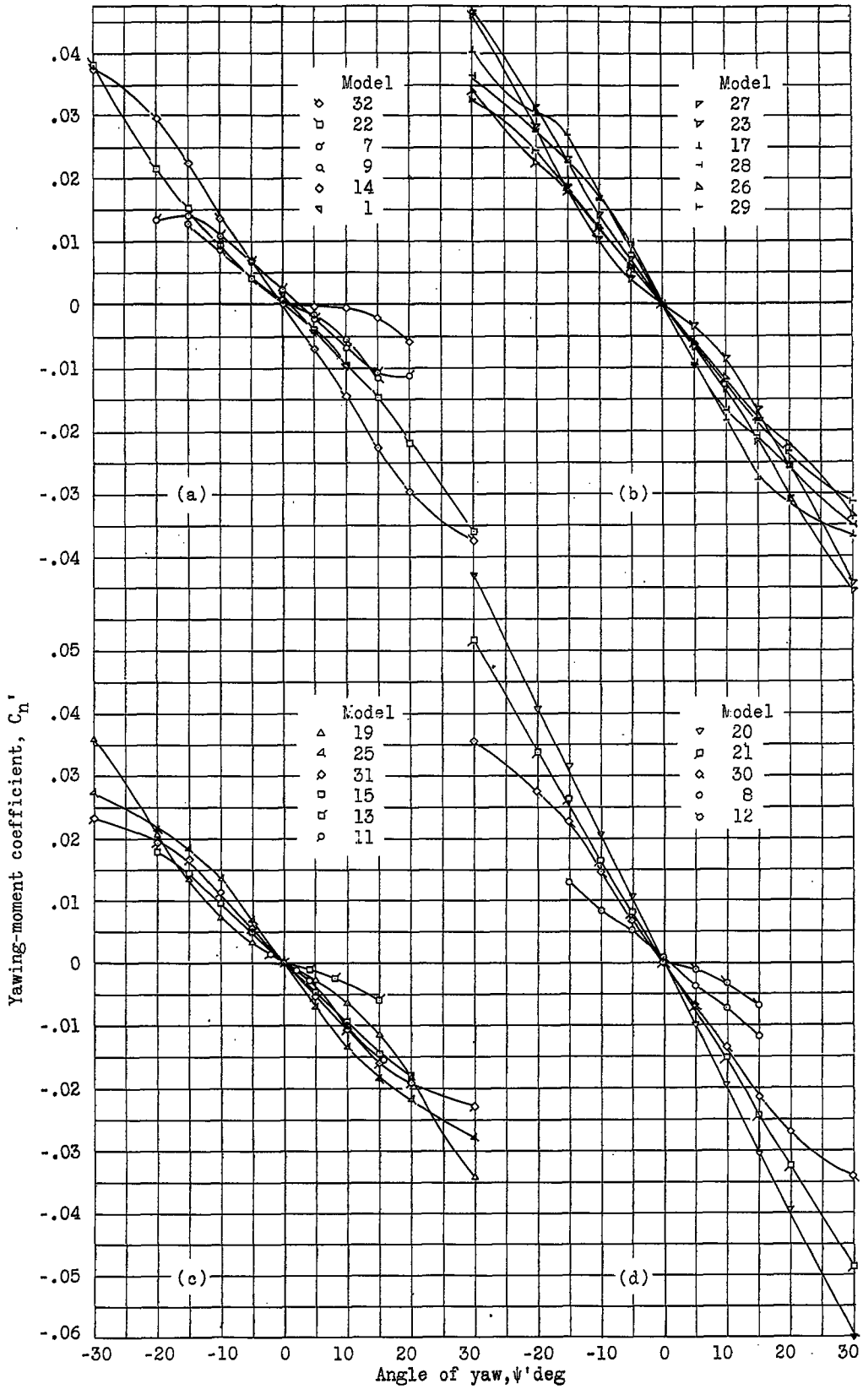

Figure 14.- Directional stability. Yawing-moment coefficient against angle of yaw.

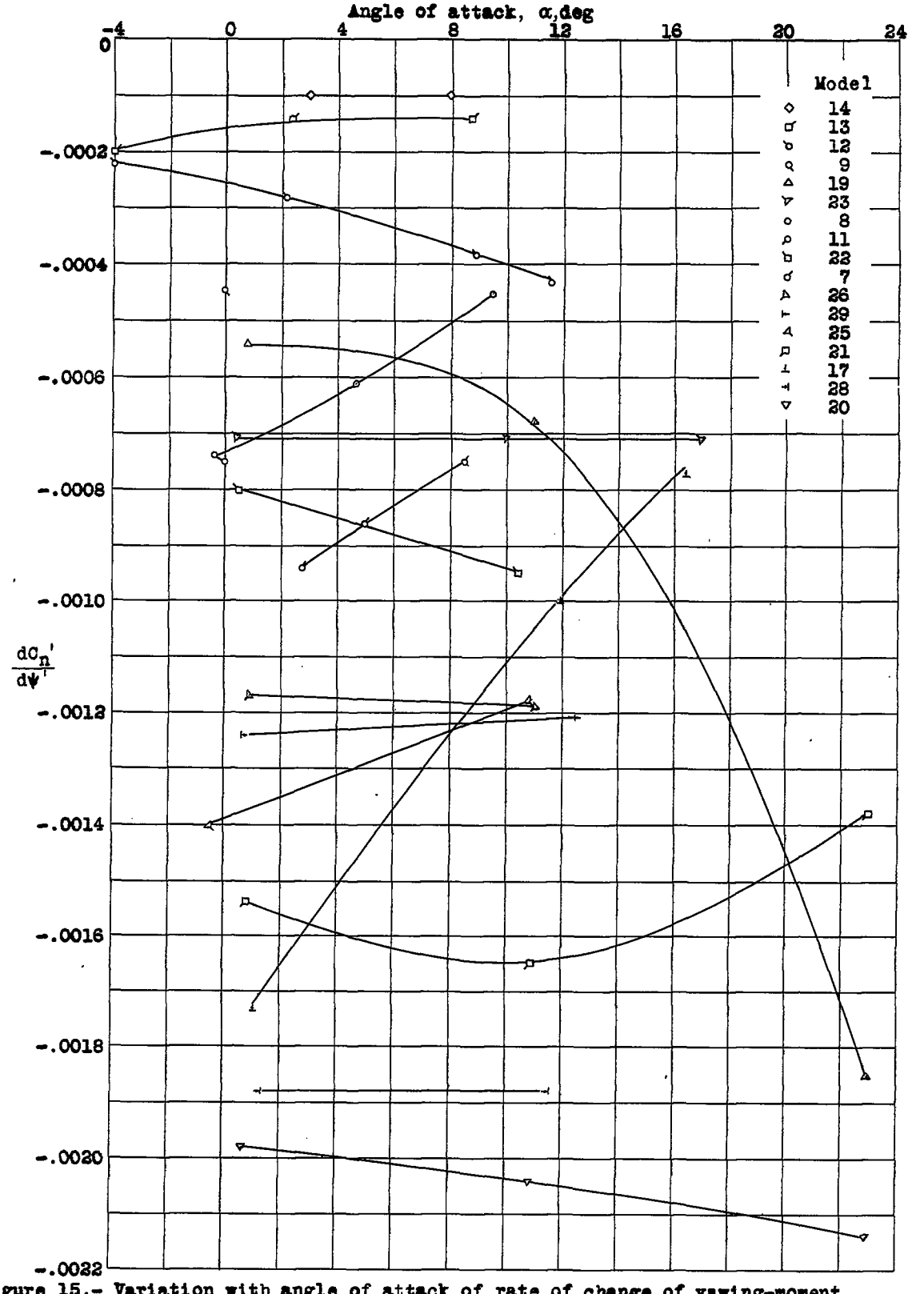

Figure 15.- Variation with angle of attack of rate of change of yawing-moment coefficient with yaw. Curves for airplanes that have poor directional stability are included; therefore, this figure cannot be used for design criterions.